

# Global Geometry of Orthogonal Foliations in the Control Allocation of Signed-Quadratic Systems

Antonio Franchi<sup>1,2</sup>

**Abstract**—This work formalizes the differential topology of redundancy resolution for systems governed by signed-quadratic actuation maps. By analyzing the minimally redundant case, the global topology of the continuous fiber bundle defining the nonlinear actuation null-space is established. The distribution orthogonal to these fibers is proven to be globally integrable and governed by an exact logarithmic potential field. This field foliates the actuator space, inducing a structural stratification of all orthants into transverse layers whose combinatorial sizes follow a strictly binomial progression. Within these layers, adjacent orthants are continuously connected via lower-dimensional strata termed reciprocal hinges, while the layers themselves are separated by boundary hyperplanes, or portals, that act as global sections of the fibers. This partition formally distinguishes extremal and transitional layers, which exhibit fundamentally distinct fiber topologies and foliation properties. Through this geometric framework, classical pseudo-linear static allocation strategies are shown to inevitably intersect singular boundary hyperplanes, triggering infinite-derivative kinetic singularities and fragmenting the task space into an exponential number of singularity-separated sectors. In contrast, allocators derived from the orthogonal manifolds yield continuously differentiable global sections with only a linear number of sectors for transversal layers, or can even form a single global diffeomorphism to the task space in the case of the two extremal layers, thus completely avoiding geometric rank-loss and boundary-crossing singularities. These theoretical results directly apply to the control allocation of propeller-driven architectures, including multirotor UAVs, marine, and underwater vehicles.

**Index Terms**—Control allocation, redundancy resolution, differential topology, singularity avoidance, redundant systems, nonlinear control systems.

## I. INTRODUCTION

The control allocation problem for redundant actuation systems requires mapping a lower-dimensional task space onto a higher-dimensional space of actuator internal states [1]. Traditionally, this is framed as a constrained optimization problem. Static Control Allocation (SCA) instantaneously distributes control effort using generalized inverses, constrained least-squares, and saturation logic, yielding comprehensive algorithmic frameworks developed extensively for aerospace and maritime domains [1, 2, 3, 4, 5, 6, 7].

In parallel, the control systems community has formalized Dynamic Control Allocation (DCA) to optimize the internal input response over time without perturbing the closed-loop

output established by a primary controller [8]. This structural augmentation relies on output invisibility—driving internal kinetic states strictly within the allocation null-space via dynamic optimization [9, 10, 11, 12] or sensitivity-based gradient methods for periodic trajectories [13]. Actively manipulating these redundant internal degrees of freedom is also the primary mechanism for fault-tolerant reallocation [14, 15] and windup mitigation [16]. Whether employing static algebraic mappings or dynamic output-invisible flows, the safe execution of any allocation algorithm intrinsically depends on navigating the unobservable geometry of the actuation system.

The physical relevance of this geometric structure extends across diverse engineering domains, which serve as primary benchmarks for redundancy resolution. While standard coplanar multirotors remain underactuated in  $SE(3)$ , their inherent input redundancy is conventionally resolved using classical Moore–Penrose pseudo-inverse mixing<sup>1</sup>. However, the demand for fully decoupled wrench generation has driven a systematic transition toward mechanically redundant, fully actuated, and omnidirectional platforms [17, 18, 19, 20, 21, 22, 23]. These systems, systematically evaluated through specific design taxonomies [24, 25, 26], continuously expand the operational envelope of redundant actuation. This structural redundancy extends to morphing platforms [27], multi-link aerial manipulators [28], and distributed modular assemblies [29, 30]. Furthermore, exploiting the null-space of these redundant configurations is a critical requirement for fault-tolerant flight and dynamic reallocation under actuator failure [31, 32, 33]. Beyond aerial robotics, similar actuation models and identical redundancy resolution challenges govern the marine domain, such as in multi-propeller surface vessels [34] and underwater vehicles [35]. However, while these diverse propeller-driven systems provide strong practical motivation, the scope of this work is strictly theoretical, focusing on the underlying system-theoretic properties rather than specific robotic applications.

In systems characterized by signed-quadratic actuation—such as the aforementioned multirotors and marine vehicles—the physical mapping between the kinetic space and the generated wrenches is strictly nonlinear and non-conformal. Current allocation methodologies generally address this by mapping the physical kinetic state into an auxiliary squared space, artificially reducing the nonlinear actuation to a linear relation to deploy established techniques like pseudo-inversion, convex

<sup>1</sup>Robotics and Mechatronics Department, Electrical Engineering, Mathematics, and Computer Science Faculty, University of Twente, The Netherlands.

<sup>2</sup>Department of Computer, Control and Management Engineering, Sapienza University of Rome, 00185 Rome, Italy. [schol@r-franchi.eu](mailto:schol@r-franchi.eu)

The work was partially funded by the European Commission Horizon Europe Framework under project Autoassess (101120732)

<sup>1</sup>As implemented in widely used open-source autopilots: [https://docs.px4.io/main/en/concept/control\\_allocation](https://docs.px4.io/main/en/concept/control_allocation); [https://github.com/nilskiefer/SVEA-PX4-Autopilot/blob/main/src/lib/control\\_allocation/control\\_allocation/ControlAllocationPseudoInverse.hpp](https://github.com/nilskiefer/SVEA-PX4-Autopilot/blob/main/src/lib/control_allocation/control_allocation/ControlAllocationPseudoInverse.hpp)

optimization, or predictive control. While these pseudo-linear strategies successfully satisfy instantaneous algebraic wrench constraints, they systematically ignore the native differential topology of the nonlinear kinetic space. By treating the allocation purely as an algebraic constraint equation, numerical solvers operate without formal knowledge of the geometric boundaries of the constant-task fibers. Consequently, when the auxiliary allocation is mapped back non-conformally to the physical actuator states, trajectories are frequently forced across singular boundary hyperplanes, inducing infinite-derivative velocity spikes and geometric rank-loss.

To address the limitations of pseudo-linear projection, this work studies redundancy resolution as a problem of differential topology. It is essential to clarify that this work does not propose a novel feedback controller or a real-time allocation algorithm. Instead, it provides the foundational mathematical footprint of the actuator space upon which such algorithms operate. By characterizing the level sets of the actuation map and integrating their orthogonal distribution, the exact global topological structure is formally established. While this theoretical baseline is requisite for the formal design of both dynamic and static allocators, the present analysis exploits this topology specifically to evaluate static mappings and prove the existence of singularity-free allocation.

The primary contributions of this work are as follows:

- 1) *Differential Topology of the Actuation Map*: The geometric structures of the signed-quadratic mapping for minimally redundant systems are formalized. It is proven that the continuous one-dimensional constant-task fibers asymptotically align with a unique central fiber, establishing the fundamental longitudinal flow of the kinetic space.
- 2) *Integrability and the Global Logarithmic Potential*: It is proven that the  $m$ -dimensional distribution orthogonal to the task fibers is globally integrable. The analysis derives the exact global logarithmic potential field whose level sets foliate the actuator space, forming exact orthogonal manifolds.
- 3) *Topological Classification of the Kinetic Space*: A structural stratification of the actuator space into *transitional* and *extremal* orthants is established. The exact boundary topologies of these regions—defining portals, folds, and reciprocal hinges—are characterized, proving that the orthogonal manifolds form a contiguous foliation across these singular boundaries. Transitional orthants are further partitioned into combinatorial groups, called *layers*, where global orthogonal sections are shown to reside.
- 4) *Pseudo-Linear Singularities and Small Singularity-Free Sub-sections*: Utilizing this topological framework, the structural limitations of standard pseudo-linear allocators are formally quantified. It is proven that such allocators strictly intersect an exponential ( $2^n - 2$ ) number of transitional orthants, inevitably forcing the system across  $(n-1)$ -dimensional boundary hyperplanes and intrinsically triggering infinite-derivative temporal singularities. Conversely, global sections of transitional layers adjacent to the extremal ones are shown to intersect a strictly linear

number ( $n$ ) of orthants. As a consequence, the task space is partitioned into only  $n$  singularity-free sub-sections, rather than the  $2^n$  sub-sections induced by pseudo-linear mappings. This establishes that each continuous, singularity-free domain within these topological sections spans an exponentially larger region of the task space, maximizing the uninterrupted footprint by a relative factor of  $2^n/n$ .

- 5) *Existence of Singularity-Free Global Allocation*: It is established that static allocators derived from the orthogonal manifolds within the extremal orthants form a global diffeomorphism to the entire unbounded task space. By excluding the pseudo-linear subspace from these regions, the framework provides a family of globally smooth, static right-inverses that permanently confine the system to a single orthant, guaranteeing the avoidance of singularities.

The remainder of this paper is organized as follows. Section II formalizes the system model and the actuation map. Section III derives the differential properties and asymptotic behavior of the constant-task fibers. Section IV establishes the integrability of the orthogonal distribution and defines the global logarithmic potential field. Section V formalizes the layer-stratification of the kinetic space orthants and constructs the global orthogonal sections and Sec. VI summarizes the discovered structures and results. Section VII leverages these topological results to compare pseudo-linear allocation against orthogonal allocation. Section VIII concludes the work.

## II. SIGNED-QUADRATIC ACTUATION MODEL

This section formalizes the algebraic and differential properties of systems governed by a signed-quadratic actuation map. The mathematical formulation presented herein is strictly agnostic to the underlying physical platform, establishing a general geometric framework for redundancy resolution.

**Definition 1** (Kinetic space and state, Task, and Signed-quadratic Actuation Map). *Let  $\mathcal{V} \cong \mathbb{R}^n$  denote the kinetic space, representing the array of  $n$  internal actuator states  $v = [v_1, \dots, v_n]^T$  (the kinetic state). Let  $\mathcal{W} \cong \mathbb{R}^m$  denote the task space of actuator outputs  $w = [w_1, \dots, w_m]^T$  (the task). A nonlinear signed-quadratic actuation system is characterized by an actuation map defined by:*

$$f : \mathcal{V} \rightarrow \mathcal{W}, \quad v \mapsto f(v) \triangleq A(v \odot |v|), \quad (1)$$

where  $A \in \mathbb{R}^{m \times n}$  is a constant allocation matrix,  $|v| = [|v_1|, \dots, |v_n|]^T$  denotes the element-wise absolute value, and  $\odot$  denotes the Hadamard (element-wise) product.

To ensure the physical realizability of arbitrary task-space commands and to isolate the native geometric properties of the map, the following structural assumption is established.

**Assumption 1** (Surjectivity and Minimal Redundancy). *The allocation matrix  $A$  is full row rank, such that  $\text{rank}(A) = m$ . Furthermore, the system is minimally redundant, possessing exactly one degree of actuation redundancy:  $n = m + 1$ .*

The restriction to the minimally redundant case is a deliberate analytical choice. As demonstrated in subsequent sections,

this  $n = m + 1$  configuration uniquely isolates the fundamental one-dimensional fiber topology of the nonlinear null-space, which fundamentally governs the broader redundancy resolution problem.

The continuous execution of a time-varying task trajectory  $w(t) \in \mathcal{W}$  requires a corresponding continuous lift  $v(t) \in \mathcal{V}$ . The relationship between the velocities in the task space and the kinetic space is governed by the differential of the actuation map,  $df_v : T_v \mathcal{V} \rightarrow T_{f(v)} \mathcal{W}$ , which is represented by the state-dependent Jacobian matrix  $J(v) = \frac{\partial f}{\partial v} \in \mathbb{R}^{m \times n}$ . This tangent-space mapping is given by:

$$\dot{w} = J(v)\dot{v}. \quad (2)$$

In practical systems, the tangent vector  $\dot{v}$  is strictly bounded by finite physical capacities (e.g.,  $\|\dot{v}\|_\infty \leq \bar{u}$ ). A kinematic singularity occurs at states  $v \in \mathcal{V}$  where a chosen right-inverse mapping from  $\mathcal{W}$  to  $\mathcal{V}$  forces the Jacobian pseudo-inverse to diverge. In such neighborhoods, maintaining a bounded task velocity  $\dot{w}$  demands an infinite kinetic velocity ( $\|\dot{v}\| \rightarrow \infty$ ). Because physical limits prohibit infinite derivatives, these topological singularities strictly bound the feasible continuous operational space. Consequently, defining the exact differential topology of  $\mathcal{V}$  to guarantee the avoidance of such boundaries is a strict prerequisite for safe control allocation.

**Remark 1** (Physical Interpretation). *While the map (1) is analyzed geometrically, it inherently models a broad class of propeller-driven architectures. In the context of multirotor UAVs or marine vehicles, the kinetic state  $v$  represents the rotor angular velocities, the task  $w$  represents the spatial wrenches (forces and moments) exerted on the rigid body, and the matrix  $A$  encapsulates the aerodynamic thrust/drag coefficients, rotor positions, and cant angles. The minimal redundancy condition  $n = m + 1$  corresponds, for example, to an fully actuated eptarotor controlling  $m = 6$  degrees of freedom, or an underactuated custom planar pentarotor controlling  $m = 4$  degrees of freedom. Furthermore, the abstract constraint  $\|\dot{v}\|_\infty \leq \bar{u}$  directly models the physical torque saturation limits of the brushless DC motors. Thus, a geometric singularity demanding  $\|\dot{v}\| \rightarrow \infty$  physically manifests as actuator windup and likely loss of control.*

### III. FIBERS TOPOLOGY AND TANGENT SPACES

Given the minimal redundancy condition  $n = m + 1$ , the level sets of the actuation map  $f(v) = w$ —that is, the  $w$ -parameterized sets  $f^{-1}(w) = \{v \in \mathbb{R}^n \mid f(v) = w\}$ —are one-dimensional continuous curves that foliate the kinetic space  $\mathcal{V}$ . We formally define the parameterization of these curves.

**Definition 2** (Transformed State and Fiber Parameterization). *Let  $g : \mathcal{V} \rightarrow \mathcal{X} \cong \mathbb{R}^n$  be the mapping defined by  $v \mapsto g(v) = v \odot |v|$  (i.e.,  $g_i(v_i) = v_i |v_i|$ ). This mapping is a global homeomorphism and a diffeomorphism everywhere except on the coordinate hyperplanes (i.e., it fails to be a diffeomorphism wherever  $\prod_{i=1}^n v_i = 0$  due to the Jacobian becoming singular). The variable  $x = g(v)$  is defined as the transformed state of  $v$  and  $\mathcal{X}$  is the transformed space, under*

which the nonlinear actuation map simplifies to the linear map  $f \circ g^{-1} : \mathcal{X} \rightarrow \mathcal{W}$  defined by  $x \mapsto Ax$ .

For any task  $w \in \mathcal{W}$ , the level set in the transformed space  $\mathcal{X}$  is the one-dimensional affine subspace  $\{z_w^A + \lambda b^A \in \mathcal{X} \mid \lambda \in \mathbb{R}\}$ , where  $z_w^A := A^+ w$  is the minimum-norm particular solution,  $A^+$  is the Moore-Penrose pseudoinverse, and  $b^A \in \ker(A) \subset \mathcal{X}$  is a unit-norm vector spanning the one-dimensional null-space.

Applying the inverse mapping  $g^{-1}(x) = \text{sign}(x) \odot \sqrt{|x|}$ , the explicit parameterization of the fiber in the native kinetic space is given by the continuous map  $\gamma : \mathcal{W} \times \mathbb{R} \rightarrow \mathcal{V}$ :

$$\gamma(w, \lambda) = \text{sign}(z_w^A + \lambda b^A) \odot \sqrt{|z_w^A + \lambda b^A|}. \quad (3)$$

By construction, it is straightforward to verify that  $f(\gamma(w, \lambda)) = w$  for all  $\lambda \in \mathbb{R}$ , confirming that the parameterized curve correctly maps to the constant task, i.e., is the fiber associated to  $w$ . Varying the scalar parameter  $\lambda$ ,  $\gamma(w, \cdot)$  traverses the single dimension of each fiber  $f^{-1}(w)$ ,  $\forall w \in \mathcal{W}$ .

To ensure the physical and mathematical well-posedness of the differential topology across the entire kinetic space, we introduce the following assumption regarding the null-space of the system.

**Assumption 2** (Strict Redundancy). *All components of the null-space generator are strictly non-zero, i.e.,  $b_i^A \neq 0$  for all  $i \in \{1, \dots, n\}$ .*

**Remark 2.** *Assumption 2 is standard and reflects a properly designed, fault-tolerant redundant actuation system. If  $b_k^A = 0$  for some rotor  $k$ , the null-space condition  $Ab^A = 0$  dictates that the remaining  $n - 1 = m$  columns of  $A$  are linearly dependent. Consequently, the allocation sub-matrix excluding actuator  $k$  would drop to rank  $m - 1$ . Physically, this would render the actuator  $k$  a critical single point of failure, as the remaining actuators would lack the actuation span required to maintain full dynamic control of the system. Thus, Assumption 2 ensures the system possesses true, fully coupled redundancy.*

#### A. The Central Fiber and Asymptotic Convergence

We now characterize the global behavior of the fiber foliation within the interior of the kinetic space orthants. For this, we study the specific parameterization of the fibers  $\gamma(w, \lambda)$  as the parameter  $\lambda$  diverges ( $|\lambda| \rightarrow \infty$ ).

**Definition 3** (Central Fiber and Extremal Orthants). *The central fiber is defined as the unique one-dimensional set corresponding to the zero-task condition,  $w = 0$ . Evaluating the inverse mapping  $\gamma(0, \lambda)$  yields:*

$$f^{-1}(0) = \left\{ \text{sign}(\lambda b^A) \odot \sqrt{|\lambda b^A|} \in \mathcal{V} \mid \lambda \in \mathbb{R} \right\}. \quad (4)$$

By defining the characteristic constant vector  $c^A := \text{sign}(b^A) \odot \sqrt{|b^A|} \in \mathcal{V}$ , the central fiber simplifies to the set  $\{\text{sign}(\lambda) \sqrt{|\lambda|} c^A \in \mathcal{V} \mid \lambda \in \mathbb{R}\}$ . Thus, the central fiber is a perfectly straight line in  $\mathcal{V}$  passing through the origin and spanned entirely by the direction  $c^A$ .

Because the central fiber is a straight line, it passes through exactly two opposing orthants in the  $n$ -dimensional  $\mathcal{V}$ , defined as the extremal orthants. Their geometry is strictly governed by the signature of the null-space generator  $b^A$ :

- The positive extremal orthant ( $\mathcal{O}^+$ ) is defined by the sign sequence  $\text{sign}(v_i) = \text{sign}(b_i^A)$  for all  $i$ . The central fiber inhabits this orthant for all  $\lambda > 0$ .
- The negative extremal orthant ( $\mathcal{O}^-$ ) is defined by the sign sequence  $\text{sign}(v_i) = -\text{sign}(b_i^A)$  for all  $i$ . The central fiber inhabits this orthant for all  $\lambda < 0$ .

**Theorem 1** (Asymptotic Convergence of Fibers). *For any constant task  $w \in \mathcal{W}$ , the Euclidean distance between the corresponding fiber  $f^{-1}(w)$  and the central fiber  $f^{-1}(0)$  vanishes asymptotically as the null-space parameter diverges. Specifically:*

$$\lim_{|\lambda| \rightarrow \infty} \|\gamma(w, \lambda) - \gamma(0, \lambda)\| = 0. \quad (5)$$

*Proof.* We evaluate the spatial distance between a point on a generic fiber  $\gamma(w, \lambda)$  and the corresponding point on the central fiber  $\gamma(0, \lambda)$  by examining their difference component-wise.

For a sufficiently large  $|\lambda|$ , the null-space component dominates the argument  $z_{w,i}^A + \lambda b_i^A$ . This has two consequences: first,  $\text{sign}(z_{w,i}^A + \lambda b_i^A) = \text{sign}(\lambda b_i^A)$ ; second, the ratio  $\frac{z_{w,i}^A}{\lambda b_i^A}$  approaches zero, guaranteeing that  $1 + \frac{z_{w,i}^A}{\lambda b_i^A} > 0$ . Because this term is strictly positive, the absolute value can be dropped when factoring out  $|\lambda b_i^A|$  from the argument of (3). Applying the first-order Taylor expansion  $\sqrt{1 + \epsilon} = 1 + \frac{1}{2}\epsilon + \mathcal{O}(\epsilon^2)$  yields:

$$\begin{aligned} \gamma_i(w, \lambda) &= \text{sign}(\lambda b_i^A) \sqrt{|\lambda b_i^A| \sqrt{1 + \frac{z_{w,i}^A}{\lambda b_i^A}}} \\ &= \gamma_i(0, \lambda) \left( 1 + \frac{z_{w,i}^A}{2\lambda b_i^A} + \mathcal{O}(|\lambda|^{-2}) \right). \end{aligned} \quad (6)$$

Distributing  $\gamma_i(0, \lambda)$  and noting that  $\frac{\gamma_i(0, \lambda)}{\lambda b_i^A} = \frac{1}{\sqrt{|\lambda b_i^A|}}$ , the spatial difference simplifies to:

$$\gamma_i(w, \lambda) - \gamma_i(0, \lambda) = \frac{z_{w,i}^A}{2\sqrt{|\lambda|} |b_i^A|} + \mathcal{O}(|\lambda|^{-3/2}). \quad (7)$$

Because the dominant residual term strictly decays proportionally to  $|\lambda|^{-1/2}$ , the component-wise difference vanishes as  $|\lambda| \rightarrow \infty$ . Thus, the Euclidean distance between the coordinate vectors universally approaches zero.  $\square$

Consequently, the central fiber  $f^{-1}(0)$  acts as a global asymptote for the entire foliation. Specifically, as  $\lambda \rightarrow \infty$ , the positive half-fibers of all sets  $f^{-1}(w)$  converge to the positive half of the central fiber within  $\mathcal{O}^+$ , and as  $\lambda \rightarrow -\infty$ , the negative half-fibers converge to the negative half of the central fiber within  $\mathcal{O}^-$ .

## B. Tangent Spaces of the Fibers

To study the global geometry of these fibers, it is instrumental to analyze the differential mapping.

**Lemma 1** (Fiber Tangent Space). *The Jacobian matrix of the actuation map  $f$  evaluated at any kinetic state  $v \in \mathcal{V}$  is:*

$$J_f(v) = \frac{\partial f}{\partial v} = 2A \text{diag}(|v_1|, \dots, |v_n|) = 2AD(v), \quad (8)$$

where  $D(v) := \text{diag}(|v_1|, \dots, |v_n|)$  acts as a local, state-dependent metric scaling matrix.

At any regular kinetic state  $v$  where  $v_i \neq 0$  for all  $i \in \{1, \dots, n\}$ , the implicit function theorem holds, and the tangent space to the fiber passing through  $v$  is a one-dimensional line explicitly spanned by the scaled null-space vector:

$$T_v f^{-1}(w) = \ker(J_f(v)) = \text{span}\{D(v)^{-1}b^A\}. \quad (9)$$

*Proof.* By the chain rule, the Jacobian is given by  $J_f(v) = A \frac{\partial g}{\partial v} = 2AD(v)$ . Because  $v_i \neq 0$  for all  $i$ , the diagonal matrix  $D(v)$  is strictly positive definite and invertible. Any vector  $\tau \in \ker(J_f(v))$  must satisfy  $2AD(v)\tau = 0$ , which implies  $D(v)\tau \in \ker(A) = \text{span}\{b^A\}$ . Consequently, it follows that  $\tau \in \text{span}\{D(v)^{-1}b^A\}$ .  $\square$

Having established the algebraic formulation of the tangent spaces in regular domains in Lemma 1 we now analyze their asymptotic behavior and their structural degeneracies at the boundaries of the kinetic orthants.

**Proposition 1** (Asymptotic Tangent Alignment). *For any constant task  $w \in \mathcal{W}$ , the tangent spaces of the fibers asymptotically align with the direction of the central fiber as the null-space parameter diverges. Specifically:*

$$\lim_{|\lambda| \rightarrow \infty} T_{\gamma(w, \lambda)} f^{-1}(w) = \text{span}\{c^A\}. \quad (10)$$

*Proof.* To evaluate the asymptotic direction of the tangent spaces given by (9), we track the components of a generic tangent vector  $t(\lambda)$  along the fiber  $\gamma(w, \lambda)$ . Substituting the explicit fiber definition  $\gamma_i(w, \lambda)$  and factoring out the dominant null-space term  $\lambda b_i^A$  from the argument yields:

$$t_i(\lambda) = \frac{b_i^A}{|\gamma_i(w, \lambda)|} = \frac{b_i^A}{\sqrt{|z_{w,i}^A + \lambda b_i^A|}} = \frac{b_i^A}{\sqrt{|\lambda b_i^A| \left| 1 + \frac{z_{w,i}^A}{\lambda b_i^A} \right|}}. \quad (11)$$

Recognizing that  $\frac{b_i^A}{\sqrt{|b_i^A|}} = \text{sign}(b_i^A) \sqrt{|b_i^A|} = c_i^A$ , the tangent component can be rewritten as:

$$t_i(\lambda) = \frac{1}{\sqrt{|\lambda|}} c_i^A \left( 1 + \frac{z_{w,i}^A}{\lambda b_i^A} \right)^{-1/2}. \quad (12)$$

As  $|\lambda| \rightarrow \infty$ , the ratio  $\frac{z_{w,i}^A}{\lambda b_i^A}$  approaches zero. By the continuity of the algebraic functions, the residual multiplier strictly converges to 1. Consequently, as the scalar factor  $1/\sqrt{|\lambda|}$  vanishes uniformly across all components  $t_i(\lambda)$  for  $i = 1, \dots, n$ , the

exact orientation of the tangent vector converges strictly to  $c^A$ .  $\square$

**Theorem 2** (Singularity Alignment at Orthant Boundaries). *Let  $I_0 \subset \{1, \dots, n\}$  denote a proper subset of indices ( $1 \leq |I_0| < n$ ) representing actuators that have halted, such that  $v_i = 0$  for  $i \in I_0$ . As a fiber approaches this orthant boundary, its tangent space asymptotically aligns entirely with the degenerate subspace spanned by the halted axes. Furthermore, for a generic single-actuator crossing ( $|I_0| = 1$ ), the fiber intersects the corresponding boundary hyperplane orthogonally.*

*Proof.* At the orthant boundaries,  $D(v)$  possesses  $|I_0|$  zeros on its main diagonal. Consequently,  $J_f(v)$  contains exactly  $|I_0|$  zero columns, dropping rank and rendering the standard implicit tangent formulation in (9) ill-posed.

To resolve this, we differentiate the explicit geometric parameterization of the fiber  $\gamma(w, \lambda)$  with respect to  $\lambda$ , see (3). Applying the chain rule yields the exact components of the parametric tangent vector:

$$\frac{\partial \gamma_i}{\partial \lambda} = \frac{b_i^A}{2\sqrt{|z_{w,i}^A + \lambda b_i^A|}}. \quad (13)$$

Suppose the actuators in  $I_0$  halt simultaneously at some parameter  $\lambda^*$ , such that  $z_{w,i}^A + \lambda^* b_i^A = 0$  for all  $i \in I_0$ . Near this boundary, the argument of the square root is  $z_{w,i}^A + \lambda b_i^A = b_i^A(\lambda - \lambda^*)$ . Substituting this into the exact derivative and factoring yields:

$$\frac{\partial \gamma_i}{\partial \lambda} = \frac{b_i^A}{2\sqrt{|b_i^A|}\sqrt{|\lambda - \lambda^*|}} = \left( \frac{1}{2\sqrt{|\lambda - \lambda^*|}} \right) c_i^A. \quad (14)$$

As  $\lambda \rightarrow \lambda^*$ , the scalar multiplier diverges to infinity. Consequently, the tangent components associated with the halted actuators ( $i \in I_0$ ) diverge proportionally to  $c_i^A$ , while the components of the actively spinning actuators ( $i \notin I_0$ ) remain strictly finite. Because the diverging components infinitely dominate the finite components, the continuous one-dimensional fiber aligns entirely with the subspace spanned by the axes of the dominating components. If  $|I_0| = 1$ , this subspace is a single coordinate axis, proving orthogonal intersection with the boundary hyperplane.  $\square$

**Corollary 1** (Kinematic Singularity at the Origin). *At the zero kinetic state  $v = 0 \in \mathcal{V}$ , the system encounters a complete kinematic singularity where  $J_f(0) = 0$ . However, by geometric continuation of the central fiber  $f^{-1}(0)$ , which is a straight line parameterized by  $\mu = \text{sign}(\lambda)\sqrt{|\lambda|}$  along  $c^A$ , the geometric tangent at the origin remains perfectly continuous and uniquely defined as:*

$$T_0 f^{-1}(0) = \text{span}\{c^A\}. \quad (15)$$

### C. Orthant Traversal and Global Topology of the Fibers

The explicit parameterization of the fibers reveals a strictly ordered traversal through the kinetic space  $\mathcal{V}$ . This trajectory dictates how the fibers navigate the orthants and coordinate hyperplanes.

**Lemma 2** (Orthant Traversal Sequence). *For any generic task  $w \in \mathcal{W}$ , the corresponding fiber  $\gamma(w, \cdot)$  is strictly monotonic component-wise. It crosses exactly  $n$  coordinate hyperplanes and traverses exactly  $n + 1$  distinct orthants without ever intersecting the same coordinate hyperplane twice.*

*Proof.* Consider the internal argument of the fiber parameterization for each actuator,  $u_i(w, \lambda) = z_{w,i}^A + \lambda b_i^A$ . This argument is a strictly linear function of the null-space parameter  $\lambda$ . Because  $b_i^A \neq 0$  for all  $i$  (Assumption 2), each kinetic state component  $v_i$  crosses zero exactly once at the critical parameter  $\lambda_i^* := -z_{w,i}^A/b_i^A$ .

Each zero crossing represents an intersection with the coordinate hyperplane  $v_i = 0$ , which separates the half-space where  $\text{sign}(v_i) = -\text{sign}(b_i^A)$  (traversed for  $\lambda < \lambda_i^*$ ) from the half-space where  $\text{sign}(v_i) = \text{sign}(b_i^A)$  (traversed for  $\lambda > \lambda_i^*$ ). Sorting these  $n$  distinct roots on  $\mathbb{R}$  identifies  $n$  unique hyperplane crossings. These  $n$  crossings divide the parametric domain  $\lambda \in \mathbb{R}$  into exactly  $n + 1$  continuous intervals, corresponding to  $n + 1$  traversed orthants out of the  $2^n$  possible orthants.  $\square$

**Remark 3** (Non-Generic Tasks and Simultaneous Crossings). *Lemma 2 relies on the generic condition that all  $n$  roots  $\lambda_i^*$  are strictly distinct. The set of non-generic tasks—where two or more roots coincide—forms a subset of measure zero in  $\mathcal{W}$ . If  $m > 1$  roots coincide at a single parameter value  $\lambda^*$ , the fiber intersects an  $(n - m)$ -dimensional stratum (the simultaneous intersection of  $m$  coordinate hyperplanes). During this measure-zero event,  $m$  coordinates change sign instantaneously, causing the fiber to “skip”  $m - 1$  intermediate orthants. Consequently, the fiber traverses  $k + 1$  orthants, where  $k < n$  is the number of strictly distinct roots.*

**Definition 4** (Transitional Orthants). *Based on Lemma 2, the initial orthant traversed for  $\lambda < \min_i\{\lambda_i^*\}$  corresponds to the negative extremal orthant  $\mathcal{O}^-$ . The final orthant traversed for  $\lambda > \max_i\{\lambda_i^*\}$  corresponds to the positive extremal orthant  $\mathcal{O}^+$ . For a generic task, the  $n - 1$  intermediate orthants traversed between  $\mathcal{O}^-$  and  $\mathcal{O}^+$  are defined as the transitional orthants. There exist  $2^n - 2$  such transitional orthants in the topology of the map, and each generic fiber with  $w \neq 0$  traverses exactly  $n - 1$  of them.*

**Proposition 2** (Strict Forward Progression). *The unidirectional traversal of any fiber is geometrically characterized by a continuous forward progression relative to the central fiber. The projection of the fiber’s tangent vector onto the central fiber direction  $c^A$  is strictly positive everywhere, ensuring the fiber never stalls or reverses direction.*

*Proof.* We evaluate the inner product of the parametric tangent vector  $\frac{\partial \gamma}{\partial \lambda}$  and the globally constant direction of the central fiber  $c^A$ :

$$\left\langle \frac{\partial \gamma}{\partial \lambda}, c^A \right\rangle = \sum_{i=1}^n \left( \frac{b_i^A}{2|v_i|} \right) \left( \frac{b_i^A}{\sqrt{|b_i^A|}} \right) = \sum_{i=1}^n \frac{(b_i^A)^2}{2|v_i| \sqrt{|b_i^A|}}. \quad (16)$$

Because  $(b_i^A)^2 > 0$  and the absolute value terms are strictly positive for  $v_i \neq 0$ , the summation is strictly positive everywhere within the interior of the orthants. Furthermore, at the intersection with any coordinate hyperplane (as  $\lambda \rightarrow \lambda_i^*$ ), the corresponding velocity component  $v_i \rightarrow 0$ , causing its associated term in the summation to diverge to  $+\infty$ . This guarantees that the forward progression is strictly maintained at the boundaries.  $\square$

Geometrically, Proposition 2 establishes that the angle between the central fiber and the tangent space of each generic fiber is strictly acute. While the generic fiber curves through the kinetic space, its progression along the longitudinal subspace spanned by  $c^A$  is monotonically increasing.

This bounded traversal fundamentally defines the mapping topology between the kinetic space  $\mathcal{V}$  and the task space  $\mathcal{W}$ , summarized as follows.

**Theorem 3** (Mapping Surjectivity of the Orthants). *The restriction of the actuation mapping  $f(v) = A(v \odot |v|)$  to either extremal orthant ( $\mathcal{O}^+$  or  $\mathcal{O}^-$ ) is globally surjective onto  $\mathcal{W}$ . Conversely, the restriction of  $f$  to any transitional orthant maps onto a limited conical sector of  $\mathcal{W}$  that strictly excludes a neighborhood of the origin.*

*Proof.* As  $\lambda \rightarrow \pm\infty$ , the signs of the state components are asymptotically governed by  $\pm \text{sign}(b_i^A)$ . Consequently, every continuous fiber universally originates in  $\mathcal{O}^-$  and terminates in  $\mathcal{O}^+$ . Because every generic task  $w \in \mathcal{W}$  generates a fiber that asymptotically occupies these two sets, both extremal orthants contain a pre-image for every  $w \in \mathcal{W}$ , proving global surjectivity.

In contrast, Lemma 2 dictates that the transitional orthants are traversed only by a proper subset of the fibers. Geometrically, any orthant is a conical set in  $\mathcal{V}$  (closed under positive scaling  $v \mapsto kv$  for  $k > 0$ ). Because the map is positively homogeneous of degree 2, meaning  $f(kv) = k^2 f(v)$ , it preserves this scale invariance; if  $w$  is in the image of an orthant, so is any positive scaling  $cw$ , proving the image is a conical sector in  $\mathcal{W}$ . Furthermore, the exact pre-image of the zero-task state ( $w = 0$ ) is the central fiber. By Definition 3, the central fiber resides fully within the extremal orthants and intersects the transitional orthants only at the origin  $v = 0$ . Thus, the image of the interior of any transitional orthant inherently excludes  $w = 0$  and, by continuity, a surrounding neighborhood in  $\mathcal{W}$ .  $\square$

Figure 1 illustrates the 1D continuous fiber bundles for four distinct allocation configurations in  $n = 2$  and  $n = 3$  kinetic spaces, encompassing symmetric, asymmetric, and skewed

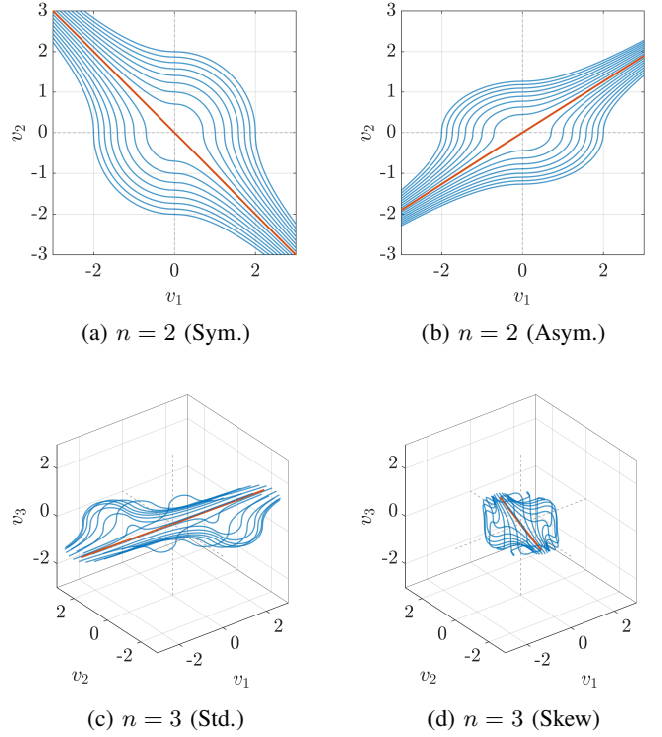


Fig. 1: The continuous fiber bundle defining the actuation null-space in the native kinetic space  $\mathcal{V}$ . The central fiber (red, thick) anchors the longitudinal flow. Adjacent fibers exhibit the expansion near the origin before asymptotically converging to and aligning with the central fiber.

geometries. This visualizes the global topological structure of the map, specifically highlighting the characteristic expansion near singular boundaries and asymptotic alignment with the central fiber. The exact allocation matrices  $A$ , normalized null-space vectors  $b^A$ , and central fiber generators  $c^A$  are detailed in Table I.

#### IV. ORTHOGONAL MANIFOLDS IN THE ORTHANTS

Having established the topological structure of the constant-task fibers  $f^{-1}(w) : \lambda \mapsto \gamma(w, \lambda)$ , we now analyze and

TABLE I: Allocation Matrices and Geometric Generators for Fig. 1

Config.	$A$	$b^A$ (Null-Space)	$c^A$ (Central Fiber)
$n = 2$ (Sym.)	$\begin{bmatrix} 1 & 1 \end{bmatrix}$	$\frac{1}{\sqrt{2}} \begin{bmatrix} -1 & 1 \end{bmatrix}^\top$	$\frac{1}{\sqrt{2}} \begin{bmatrix} -1 & 1 \end{bmatrix}^\top$
$n = 2$ (Asym.)	$\begin{bmatrix} 1 & -2.5 \end{bmatrix}$	$\frac{1}{\sqrt{29}} \begin{bmatrix} 5 & 2 \end{bmatrix}^\top$	$\frac{1}{\sqrt{29}} \begin{bmatrix} \sqrt{5} & \sqrt{2} \end{bmatrix}^\top$
$n = 3$ (Std.)	$\begin{bmatrix} 1 & 1 & 1 \\ 1 & 2 & 3 \end{bmatrix}$	$\frac{1}{\sqrt{6}} \begin{bmatrix} 1 & -2 & 1 \end{bmatrix}^\top$	$\frac{1}{\sqrt{6}} \begin{bmatrix} 1 & -\sqrt{2} & 1 \end{bmatrix}^\top$
$n = 3$ (Skew)	$\begin{bmatrix} 2 & -1 & 1 \\ 1 & 3 & 2 \end{bmatrix}$	$\frac{1}{\sqrt{83}} \begin{bmatrix} -5 & -3 & 7 \end{bmatrix}^\top$	$\frac{1}{\sqrt{83}} \begin{bmatrix} -\sqrt{5} & -\sqrt{3} & \sqrt{7} \end{bmatrix}^\top$

discover the existence and topology of  $m$ -dimensional manifolds orthogonal to these fibers. Navigating these orthogonal manifolds represents the purely task-actuating motions of the system in  $\mathcal{W}$ , while moving strictly along the fibers represents internal ‘null-space’ reconfigurations in  $\mathcal{V}$ , which are ‘invisible’ in  $\mathcal{W}$ .

#### A. Integrability and the Global Logarithmic Potential

At any regular kinetic state  $v \in \mathcal{V}$  (where  $v_i \neq 0$  for all  $i$ ), the tangent space to the one-dimensional fiber is given by (9). We seek to define an  $m$ -dimensional manifold  $\mathcal{M}$  passing through  $v$  that is strictly orthogonal to the fibers at every point. The tangent space of  $\mathcal{M}$  at  $v$  must satisfy:

$$T_v \mathcal{M} = \ker(J_f(v))^\perp = \text{Im}(J_f^T(v)) = \text{span}\{D(v)A^T\}. \quad (17)$$

In differential geometric terms, finding this manifold equates to integrating the distribution of the  $m$ -dimensional vector spaces  $T_v \mathcal{M}$  orthogonal to the fibers.

**Remark 4.** Exploiting the presence of the standard metric in  $\mathbb{R}^n$ , we algebraically treat tangent spaces and cotangent spaces as residing in  $\mathbb{R}^n$ , with their dual product operating as the standard inner product.

**Theorem 4** (Integrability of the Orthogonal Distribution). *The distribution of vector spaces orthogonal to the fibers,  $\Delta(v) = \ker(J_f(v))^\perp$ , is globally integrable on  $\mathbb{R}^n \setminus \{v_i = 0\}$ . The resulting integral manifolds are uniquely defined by the level sets of a global, exact scalar potential field  $\Phi : \mathbb{R}^n \setminus \{v_i = 0\} \rightarrow \mathbb{R}$ , given by:*

$$\Phi(v) = \sum_{i=1}^n b_i^A \text{sign}(v_i) \ln |v_i|. \quad (18)$$

*Proof.* For a differential state displacement  $dv \in \mathbb{R}^n$  to be strictly orthogonal to the fiber at  $v$ , its inner product with the fiber’s tangent vector must vanish:

$$\langle dv, D(v)^{-1}b^A \rangle = 0 \implies \sum_{i=1}^n b_i^A \frac{dv_i}{|v_i|} = 0. \quad (19)$$

Because the  $i$ -th term of this sum depends exclusively on the  $i$ -th coordinate  $v_i$ , the differential form is exact. Integrating the differential equation component-wise yields the exact, global potential function  $\Phi(v)$  in (18), proving that the distribution forms well-defined, continuous global manifolds rather than a non-holonomic vector field.  $\square$

**Definition 5** (Orthogonal Manifolds). *The orthogonal manifolds are defined as the level sets  $\mathcal{M}_C = \{v \in \mathbb{R}^n \setminus \{v_i = 0\} \mid \Phi(v) = C\}$  for any constant  $C \in \mathbb{R}$ . Because the gradient  $\nabla \Phi(v) = D(v)^{-1}b^A$  never vanishes or explodes for any finite  $v$  in the interior of an orthant (as  $b_i^A \neq 0$ ), the level sets  $\mathcal{M}_C$  form a non-intersecting foliation of the open kinetic space, where each  $\mathcal{M}_C$  is an  $m$ -dimensional smooth manifold.*

#### B. Transverse Foliation and Boundary Limits

We now establish the algebraic relationship between the orthogonal manifold level  $C$  and the internal ‘null-space’ parameter  $\lambda$  of a given fiber. Substituting the explicit fiber parameterization  $\gamma(w, \lambda)$  from (3) into the global potential function (18) yields the constant  $C$  of the exact orthogonal manifold pierced by the fiber at a given  $\lambda$ :

$$C_w(\lambda) := \Phi(\gamma(w, \lambda)) = \frac{1}{2} \sum_{i=1}^n b_i^A \text{sign}((z_w^A)_i + \lambda b_i^A) \ln |(z_w^A)_i + \lambda b_i^A|. \quad (20)$$

**Proposition 3** (Transverse Foliation and Monotonicity). *Within the interior of any orthant of  $\mathcal{V}$ , the scalar potential evaluated along a fiber,  $C_w(\lambda)$ , is strictly monotonically increasing with respect to  $\lambda$ . Consequently, each orthogonal manifold crosses every continuous fiber exactly once within a given orthant.*

*Proof.* The derivative of  $C_w$  with respect to  $\lambda$  is computed via the chain rule,  $\frac{dC_w}{d\lambda} = \sum_{i=1}^n \frac{\partial \Phi}{\partial v_i} \frac{dv_i}{d\lambda}$ . Given  $\frac{\partial \Phi}{\partial v_i} = \frac{b_i^A}{|v_i|}$  and the local tangent component  $\frac{dv_i}{d\lambda} = \frac{b_i^A}{2|v_i|}$  derived from (3), we obtain:

$$\frac{dC_w}{d\lambda} = \sum_{i=1}^n \frac{(b_i^A)^2}{2v_i^2} > 0. \quad (21)$$

Because  $b_i^A \neq 0$  and  $v_i \neq 0$  in the interior, this derivative is strictly positive, guaranteeing strict monotonicity.  $\square$

While Proposition 3 establishes local monotonicity, the global topology of the foliation is strictly governed by the boundary conditions at the coordinate hyperplanes.

**Theorem 5** (Potential Limits at Orthant Boundaries). *Let a fiber  $\gamma(w, \cdot)$  traverse a generic transitional orthant, entering at parameter  $\lambda_{in}$  across the hyperplane  $v_j = 0$ , and exiting at  $\lambda_{out} > \lambda_{in}$  across the hyperplane  $v_k = 0$ . The potential function spans the entire real line within this single orthant:  $\lim_{\lambda \rightarrow \lambda_{in}^+} C_w(\lambda) = -\infty$  and  $\lim_{\lambda \rightarrow \lambda_{out}^-} C_w(\lambda) = +\infty$ .*

*Proof.* At the entry boundary ( $\lambda \rightarrow \lambda_{in}^+$ ), the transformed coordinate  $x_j(\lambda) = (z_w^A)_j + \lambda b_j^A$  departs from zero. Because the fiber advances monotonically,  $x_j$  immediately assumes the sign of its directional slope,  $b_j^A$ . Thus, just inside the new orthant,  $\text{sign}(v_j) = \text{sign}(b_j^A)$ . The  $j$ -th term of the potential becomes  $|b_j^A| \ln |v_j|$ . As  $|v_j| \rightarrow 0$ ,  $\ln |v_j| \rightarrow -\infty$ , dominating the sum and yielding  $-\infty$ .

Conversely, as the fiber approaches the exit boundary ( $\lambda \rightarrow \lambda_{out}^-$ ),  $x_k(\lambda)$  approaches zero from a non-zero value. Because  $\lambda$  is strictly increasing,  $x_k$  is moving in opposition to its slope  $b_k^A$ , imposing  $\text{sign}(v_k) = -\text{sign}(b_k^A)$ . The  $k$ -th term in the potential becomes  $-|b_k^A| \ln |v_k|$ . As  $|v_k| \rightarrow 0$ , the logarithmic divergence is inverted by the sign coefficient, forcing the sum to  $+\infty$ .  $\square$

Geometrically, Theorem 5 governs the asymptotic behavior of the orthogonal manifolds near the orthant boundaries. While

the isolated vanishing of a single kinetic state coordinate forces the manifold to flatten as its potential diverges, it does not inherently compromise the system's control authority. In contrast, any continuous trajectory strictly confined to a specific orthogonal manifold (maintaining a constant, finite potential  $C$ ) precludes such isolated vanishing; the logarithmic divergence must be balanced by at least one additional coordinate approaching zero with an opposing sign coefficient. This mandatory simultaneous vanishing fundamentally restricts the tangent space geometry at the boundary intersections, ultimately inducing a strict kinematic singularity. These exact geometric and algebraic consequences are formalized in the following corollaries.

**Corollary 2** (Flattening of the Orthogonal Manifold). *As a single coordinate  $v_i$  of the kinetic state  $v$  tends to 0, the orthogonal manifold passing through  $v$  asymptotically flattens to become parallel to the bounding hyperplane  $v_i = 0$ , while its corresponding potential diverges,  $|C| \rightarrow \infty$ . Note that the vanishing of a single coordinate does not induce a singularity; the Jacobian in (8) remains full rank by virtue of Assumption 2 and thus it is possible to select  $\dot{v}$  parallel to the bounding hyperplane while generating all possible velocities in  $T_{f(v)}\mathcal{W}$ .*

**Corollary 3** (Geometric Boundary Alignment). *For a continuous path confined to an orthogonal manifold of finite potential  $C$ , the approach to a bounding hyperplane  $v_i \rightarrow 0$  necessitates the simultaneous vanishing of at least one additional coordinate  $v_j \rightarrow 0$  ( $j \neq i$ ). In the limit as  $k \geq 2$  coordinates simultaneously vanish, the corresponding components of the gradient  $\nabla\Phi = D(v)^{-1}b^A$  diverge. Consequently, the normal vector of the manifold aligns entirely within the  $k$ -dimensional subspace of the vanishing coordinates. The  $m$ -dimensional tangent space of the manifold therefore strictly aligns to contain the  $(n-k)$ -dimensional intersection of those bounding hyperplanes, with its remaining dimensions extending outward into the interior of the orthant.*

**Corollary 4** (Kinematic Singularity at the Boundary). *The necessary simultaneous vanishing of  $k \geq 2$  coordinates at the boundary of the orthogonal manifolds, as dictated by Corollary 3, causes the Jacobian in (8) to lose rank. This rank deficiency constitutes a kinematic singularity of the nonlinear mapping, locally precluding the instantaneous assignment of task velocities  $\dot{w}$  within a  $(k-1)$ -dimensional subspace of the tangent space  $T_{f(v)}\mathcal{W}$ .*

### C. Topology of the Orthogonal Foliation for Transitional Orthants

To formally characterize the global evolution of the orthogonal manifolds  $\mathcal{M}_C$  and their interaction with the task fibers  $\gamma(w, \lambda)$ , we partition the boundary of any transitional orthant into functional sets. Let  $\mathcal{O}_\sigma$  be a transitional orthant defined by the sign vector  $\sigma \in \{-1, 1\}^n$ , with boundary faces defined as  $F_\sigma^k = \{v \in \partial\mathcal{O}_\sigma \mid v_k = 0\}$ .

**Definition 6** (Portals, Hinges, and Folds). *Based on the mapping of the null-space vector  $b^A$ , the coordinate indices*

$k \in \{1, \dots, n\}$  within  $\mathcal{O}_\sigma$  are partitioned into an entry set  $\mathcal{I}_\sigma^{in} = \{i \mid \sigma_i b_i^A > 0\}$  and an exit set  $\mathcal{I}_\sigma^{out} = \{j \mid \sigma_j b_j^A < 0\}$ .

We define the entry portal  $\mathcal{P}_\sigma^{in}$  and the exit portal  $\mathcal{P}_\sigma^{out}$  as the unions of their respective boundary faces:

$$\mathcal{P}_\sigma^{in} = \bigcup_{i \in \mathcal{I}_\sigma^{in}} F_\sigma^i, \quad \mathcal{P}_\sigma^{out} = \bigcup_{j \in \mathcal{I}_\sigma^{out}} F_\sigma^j. \quad (22)$$

The lower-dimensional strata formed by the intersections of these faces are partitioned into two distinct geometric classes:

- 1) The orthant hinges  $\mathcal{H}_\sigma$ : The intersections between entry and exit faces, defined as  $\mathcal{H}_\sigma = \mathcal{P}_\sigma^{in} \cap \mathcal{P}_\sigma^{out}$ .
- 2) The portal folds  $\mathcal{S}_\sigma^{in}$  and  $\mathcal{S}_\sigma^{out}$ : The face intersections contained entirely within a single portal, lacking any hinge component. For example, the entry folds are defined as  $\mathcal{S}_\sigma^{in} = \bigcup_{i \neq k \in \mathcal{I}_\sigma^{in}} (F_\sigma^i \cap F_\sigma^k) \setminus \mathcal{H}_\sigma$ .

**Theorem 6** (Topological Sweep of the Orthogonal Foliation). *For any transitional orthant  $\mathcal{O}_\sigma$ , the task fibers  $\gamma(w, \lambda)$  and the orthogonal manifolds  $\mathcal{M}_C$  exhibit the following topological properties:*

- 1) Every fiber that traverses the interior of  $\mathcal{O}_\sigma$  enters strictly through  $\mathcal{P}_\sigma^{in}$  (including its folds  $\mathcal{S}_\sigma^{in}$ ) and exits strictly through  $\mathcal{P}_\sigma^{out}$  (including  $\mathcal{S}_\sigma^{out}$ ). Fibers intersecting the hinges  $\mathcal{H}_\sigma$  are strictly tangent to  $\bar{\mathcal{O}}_\sigma$  and map to the task-space boundary of achievable tasks  $\partial\mathcal{W}_\sigma$  for that specific orthant.
- 2) For any finite scalar  $C \in \mathbb{R}$ , the boundary of the orthogonal manifold  $\mathcal{M}_C$  is asymptotically anchored entirely and exclusively to the hinges  $\mathcal{H}_\sigma$ .
- 3) As  $C \rightarrow -\infty$ , the manifold  $\mathcal{M}_C$  asymptotically flattens against the entry portal  $\mathcal{P}_\sigma^{in}$ . As  $C \rightarrow +\infty$ ,  $\mathcal{M}_C$  asymptotically flattens against the exit portal  $\mathcal{P}_\sigma^{out}$ , continuously sweeping the entire interior of the orthant. During this asymptotic flattening, the manifolds develop geometric creases along the portal folds ( $\mathcal{S}_\sigma^{in}$  and  $\mathcal{S}_\sigma^{out}$ ) to attain contiguous adherence to the multi-faced portals.

*Proof.* We prove the three claims sequentially.

1) Let a fiber be parameterized by  $\lambda$ , mapping to the transformed state  $x_k(\lambda) = (z_k^A)_k + \lambda b_k^A$ . For a fiber to enter  $\mathcal{O}_\sigma$  across a face  $F_\sigma^k$ , the coordinate must transition to match the orthant sign  $\sigma_k$ , requiring  $\text{sign}(dx_k/d\lambda) = \text{sign}(b_k^A) = \sigma_k$ . This precisely satisfies the condition for  $\mathcal{I}_\sigma^{in}$ , proving entry occurs exclusively through  $\mathcal{P}_\sigma^{in}$ . Conversely, exiting satisfies the condition for  $\mathcal{I}_\sigma^{out}$ .

Now, consider a fiber intersecting a hinge at  $h \in \mathcal{H}_\sigma$  at some parameter  $\lambda^*$ . By definition of  $\mathcal{H}_\sigma$ , there exists at least one entry index  $i \in \mathcal{I}_\sigma^{in}$  and one exit index  $j \in \mathcal{I}_\sigma^{out}$  such that  $x_i(\lambda^*) = x_j(\lambda^*) = 0$  simultaneously. For any infinitesimal progression  $\lambda > \lambda^*$ , the entry coordinate  $x_i$  transitions to match  $\sigma_i$ . However, because  $j \in \mathcal{I}_\sigma^{out}$ , the exit coordinate  $x_j$  strictly transitions away from  $\sigma_j$ . Therefore, for all  $\lambda \neq \lambda^*$ , the fiber violates the strict sign condition of  $\mathcal{O}_\sigma$ . The fiber remains entirely outside the orthant interior, intersecting it tangentially without penetrating. These tangent fibers define the geometric boundary  $\mathcal{W}_\sigma = \partial f(\mathcal{O}_\sigma)$  in the task-space, separating the

tasks  $w \in f(\mathcal{O}_\sigma)$  that are achievable by a kinetic state  $v \in \mathcal{O}_\sigma$  from those that do not. At folds  $S_\sigma^{in}$ , all intersecting faces belong to  $\mathcal{I}_\sigma^{in}$ ; thus, all concurrent zero-crossings transition into the correct orthant signs simultaneously, permitting valid entry. Similarly for  $S_\sigma^{out}$  regarding the exit.

2) The orthogonal manifolds inside  $\mathcal{O}_\sigma$  are defined by the level sets of the potential function:

$$\Phi(v) = \sum_{i \in \mathcal{I}_\sigma^{in}} |b_i^A| \ln |v_i| - \sum_{j \in \mathcal{I}_\sigma^{out}} |b_j^A| \ln |v_j| = C. \quad (23)$$

Consider the limit as the manifold approaches an entry face  $F_\sigma^i$  (where  $v_i \rightarrow 0$ ) for a fixed, finite  $C$ . The corresponding entry logarithmic term diverges to  $-\infty$ . To satisfy the potential equation  $\Phi(v) = C$ , the exit summation must correspondingly diverge to  $-\infty$ , which strictly requires at least one exit coordinate  $v_j \rightarrow 0$  (approaching face  $F_\sigma^j$ ). Therefore, the limits of the manifold exist only where  $v_i = 0$  and  $v_j = 0$  simultaneously, which precisely defines the hinges  $\mathcal{H}_\sigma = F_\sigma^i \cap F_\sigma^j$ .

3) Let  $C \rightarrow -\infty$ . To satisfy the potential equation, the strictly positive summation over the entry set in (23) must dominate, forcing  $\sum_{i \in \mathcal{I}_\sigma^{in}} |b_i^A| \ln |v_i| \rightarrow -\infty$ . This requires the manifold to be arbitrarily close to the entry faces, meaning  $\mathcal{M}_{-\infty} \rightarrow \mathcal{P}_\sigma^{in}$ . Because  $\mathcal{P}_\sigma^{in}$  is the union of multiple intersecting hyperplanes, a single continuous manifold flattening against it must conform to its piecewise-linear topology. Consequently, the manifold creases along the intersection loci of these faces, mapping perfectly to the pure entry folds  $S_\sigma^{in}$ . By symmetry, as  $C \rightarrow +\infty$ , the subtracted exit sum in (23) dominates, forcing  $\mathcal{M}_{+\infty} \rightarrow \mathcal{P}_\sigma^{out}$ , and the manifold creases along  $S_\sigma^{out}$ . Because  $\Phi(v)$  is continuous and monotonically increasing along any valid transversing fiber (Proposition 3), the manifolds continuously sweep the entire volume of  $\mathcal{O}_\sigma$  between these asymptotic bounds.  $\square$

#### D. Topology of the Orthogonal Foliation for Extremal Orthants and Asymptotic Divergence

The topological behavior defined for transitional orthants shifts fundamentally when considering an extremal orthant. An orthant is defined as extremal if its sign vector  $\sigma$  perfectly matches (the positive orthant  $\mathcal{O}^+$ ) or perfectly opposes (the negative orthant  $\mathcal{O}^-$ ) the signs of the null-space mapping vector  $b^A$ .

**Theorem 7** (Topological Sweep in Extremal Orthants). *In the extremal orthants  $\mathcal{O}^+$  and  $\mathcal{O}^-$ , there are no hinges ( $\mathcal{H}^+ = \mathcal{H}^- = \emptyset$ ). Furthermore,  $\mathcal{O}^+$  possesses no exit portals ( $\mathcal{P}_+^{out} = \emptyset$ ), and  $\mathcal{O}^-$  possesses no entry portals ( $\mathcal{P}_-^{in} = \emptyset$ ). For any constant finite  $C$ , the orthogonal manifolds  $\mathcal{M}_C$  do not converge asymptotically to any hinge. Instead, as  $C$  varies, the manifolds sweep the entire infinite volume of the orthant: they asymptotically flatten against the bounding portals in one limit of  $C$ , and expand with unbounded divergence toward spatial infinity in the opposite limit.*

*Proof.* In an extremal orthant, all components of the product  $\sigma_k b_k^A$  share the same strict sign. Consequently, all boundary

faces belong exclusively to the entry portal  $\mathcal{P}_\sigma^{in}$  for  $\mathcal{O}^+$  (where  $\sigma_k b_k^A > 0$ ) or exclusively to the exit portal  $\mathcal{P}_\sigma^{out}$  for  $\mathcal{O}^-$  (where  $\sigma_k b_k^A < 0$ ). The opposing portal is inherently empty, which strictly implies the intersection set is empty:  $\mathcal{H}_\sigma = \mathcal{P}_\sigma^{in} \cap \mathcal{P}_\sigma^{out} = \emptyset$ .

Consider the extremal orthant  $\mathcal{O}^+$ , where the exit portal is empty ( $\mathcal{P}_+^{out} = \emptyset$ ). Within this orthant, the potential function evaluates as a strictly positively weighted sum of logarithms:  $\Phi(v) = \sum_{i=1}^n |b_i^A| \ln |v_i| = C$ .

To formalize the limit  $C \rightarrow -\infty$ , consider an arbitrary  $v^* \in \mathcal{P}_+^{in}$ . By definition of the boundary,  $v^*$  possesses at least one vanishing coordinate,  $v_k^* = 0$ . For any sequence of interior points  $v^{(m)} \rightarrow v^*$ , the corresponding term  $|b_k^A| \ln |v_k^{(m)}| \rightarrow -\infty$ . Because all other logarithmic terms are bounded from above in any finite neighborhood of  $v^*$ , the total potential strictly diverges to  $-\infty$ . Since this holds for every point  $v^* \in \mathcal{P}_+^{in}$ , the level set  $\mathcal{M}_C$  asymptotically converges to and entirely covers the portal as  $C \rightarrow -\infty$ .

Conversely, to formalize the limit  $C \rightarrow +\infty$ , consider an arbitrary open ray strictly within the interior of the orthant, parameterized by  $v(r) = ru$ , where  $u \in \text{int}(\mathcal{O}^+)$  is a constant directional vector and  $r > 0$ . Evaluating the potential along this ray yields:

$$\Phi(ru) = \left( \sum_{i=1}^n |b_i^A| \right) \ln r + \sum_{i=1}^n |b_i^A| \ln u_i. \quad (24)$$

Because  $u$  lies strictly in the interior,  $u_i > 0$  for all  $i$ , making the second sum a finite constant. As the radial distance  $r \rightarrow \infty$ , the strictly positive coefficient  $\sum |b_i^A| > 0$  guarantees that  $\Phi(ru) \rightarrow +\infty$ . Because this strict radial divergence applies along *any* arbitrary interior direction  $u$ , the sequence of manifolds  $\mathcal{M}_C$  expands uniformly outward in all directions, encompassing all points at spatial infinity as  $C \rightarrow +\infty$ .  $\square$

The geometric appearance of the orthogonal manifolds in low-dimensional cases is visualized in Fig. 2. In the transitional orthants (Fig. 2b and 2c), the mixed signs of the potential field coefficients force the limit cases  $C \rightarrow -\infty$  and  $C \rightarrow +\infty$  onto distinct, non-adjacent boundary hyperplanes. This forms distinct ‘entry’ and ‘exit’ portals, allowing the kinetic fibers to fully traverse the orthant. In the extremal orthants shown in Fig. 2a and 2d, all the hyperplanes bounding the orthant are part of a unique entry portal to which the manifolds converge as  $C \rightarrow -\infty$ . In this case, the manifolds foliate the full orthant, sweeping through it in the direction of the central fiber as  $C \rightarrow +\infty$ .

#### E. The Two Algebraic Varieties of Orthogonal Manifolds

To classify the geometric shapes generated in the two cases demonstrated before, we transform the logarithmic potential into an algebraic variety.

**Proposition 4** (Algebraic Representation of Orthogonal Manifolds). *For any finite  $C \in \mathbb{R}$ , the orthogonal manifold  $\mathcal{M}_C$  can be explicitly represented as an algebraic equation.*

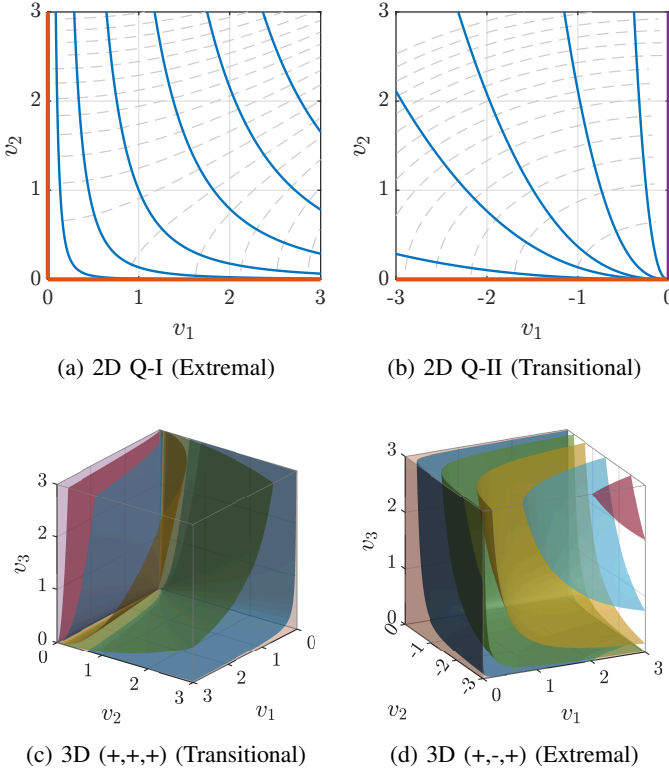


Fig. 2: Level sets of the global logarithmic potential field defining the orthogonal manifolds. The top row utilizes the  $n = 2$  asymmetric allocation map from Fig. 1b, showing the family of curves for  $C \in \{-10, -4, 0, 35, 6.5\}$  in the extremal Quadrant I and  $C \in \{-8, -4, -2, 1.5, 7\}$  in the transitional Quadrant II. The bottom row utilizes the  $n = 3$  standard allocation from Fig. 1c, illustrating the surfaces for  $C \in \{-5, -1.5, 0.5, 2.5, 5\}$  in the transitional  $(+, +, +)$  octant and  $C \in \{-4, -0.5, 1.5, 3, 4\}$  in the extremal  $(+, -, +)$  octant. Thick colored boundaries denote the limit cases  $C \rightarrow \pm\infty$ , highlighting the difference between entry and exit portals in the transitional and extremal orthants. When present, background dashed lines indicate the fibers.

Let  $K = e^C$ , where  $K > 0$ . Exponentiating the potential  $\Phi(v) = C$  yields:

$$\prod_{i \in \mathcal{I}_{\sigma}^{in}} |v_i|^{b_i^A} = K \prod_{j \in \mathcal{I}_{\sigma}^{out}} |v_j|^{b_j^A}. \quad (25)$$

*Proof.* By applying the exponential function to both sides of (18), the summation of logarithms transforms into a product of powers:  $\prod_{k=1}^n |v_k|^{\sigma_k b_k^A} = K$ . Separating this product into the entry set  $\mathcal{I}_{\sigma}^{in}$  (where  $\sigma_i b_i^A = |b_i^A|$ ) and the exit set  $\mathcal{I}_{\sigma}^{out}$  (where  $\sigma_j b_j^A = -|b_j^A|$ ) produces a fractional algebraic relation. Multiplying by the denominator yields the exact equality in (25).  $\square$

This explicit formulation classifies the orthogonal manifolds into two distinct algebraic families, strictly dictated by the topological class of the orthant.

**Corollary 5** (Geometric Classification of the Foliation). *Based on Proposition 4, the foliation geometry within a given orthant is classified into two distinct generalized families:*

- 1) **Extremal Orthants (Hyperbolic):** *Because one index set is empty (e.g.,  $\mathcal{I}_{\sigma}^{out} = \emptyset$ ), (25) reduces to a single monomial of same-sign terms:  $\prod_i |v_i|^{b_i^A} = K$ . This defines a generalized hyperbolic hypersurface. As  $K \rightarrow 0$  ( $C \rightarrow -\infty$ ), the hyperbola asymptotically collapses onto the coordinate hyperplanes comprising the single portal. As  $K \rightarrow \infty$  ( $C \rightarrow +\infty$ ), the hyperbolic surface expands outward, diverging toward spatial infinity without bounded intersection.*
- 2) **Transitional Orthants (Saddle/Hyperbolic Paraboloid):** *Because both entry and exit sets are populated, (25) equates a monomial of entry coordinates to a monomial of exit coordinates. This defines a generalized saddle hypersurface (a generalized hyperbolic paraboloid). This multiplicative balance forces the manifold to remain permanently anchored at the singular hinges (where  $v_i = v_j = 0$  satisfies  $0 = K \cdot 0$  for all  $K$ ), while allowing the interior of the saddle to continuously pivot between the entry and exit portals as  $K$  varies across  $(0, \infty)$ .*

## V. LAYER PARTITION OF THE ORTHANTS AND GLOBAL ORTHOGONAL SECTIONS

### A. The Stratified Layer Partition of Orthants

The global topology of the task fibers implies a highly structured partitioning of the transitional orthants in the  $n$ -dimensional kinetic space  $\mathcal{V}$  which are organized into distinct layers based on their progression between the two extremal orthants. To formalize this stratification, consider the transformed coordinate mapping of a generic fiber:  $x_k(\lambda) = (z_w^A)_k + \lambda b_k^A$ . Because this function is strictly linear with respect to  $\lambda$ , each coordinate  $x_k$  must cross zero exactly once as  $\lambda$  sweeps from  $-\infty$  to  $+\infty$ . Consequently, every coordinate changes its sign relative to the null-space vector exactly once along any valid fiber. Traveling along a continuous fiber from  $\lambda \rightarrow -\infty$  to  $\lambda \rightarrow +\infty$  is therefore combinatorially equivalent to starting with a kinetic state entirely opposite in sign to  $b^A$  and flipping the signs one by one until they are entirely aligned with  $b^A$ . This strict monotonic progression allows the  $2^n$  orthants to be grouped by the number of signs that have successfully transitioned. The initial negative extremal orthant  $\mathcal{O}^-$  possesses  $n$  exit faces and 0 entry faces. As a fiber crosses a boundary face into a subsequent orthant, exactly one exit face transitions into an entry face.

This structural grouping dictates the geometric boundaries shared by orthants within the same progressive stage. If two distinct orthants  $\mathcal{O}_{\sigma_a}$  and  $\mathcal{O}_{\sigma_b}$  possess the exact same number of entry boundary faces i.e.  $|\mathcal{I}_{\sigma_a}^{in}| = |\mathcal{I}_{\sigma_b}^{in}|$ , their signatures  $\sigma_a$  and  $\sigma_b$  cannot differ by just a single sign; changing one sign would alter their entry-face count, placing them in different stages of the fiber progression. To maintain the same count,  $\sigma_a$  and  $\sigma_b$  must differ by exactly two indices: one strictly transitioning from entry to exit, and the other from exit to entry. Because these two orthants differ by two signs rather than one, they bypass each other's  $(n-1)$ -dimensional flat faces entirely. Instead, they intersect exclusively at an  $(n-2)$ -dimensional bounding strata (e.g., an edge in  $\mathbb{R}^3$ ). Because

the two coordinates defining this intersection consist of an entry/exit pair, this bounding strata matches the geometric definition of a hinge. This leads us to the following definition.

**Definition 7** (Orthant Layers and Reciprocal Hinges). *The kinetic space orthants are partitioned into orthant layers  $\mathcal{L}_l$ , where the integer  $l \in \{0, \dots, n\}$  represents the exact number of acquired entry faces,  $\mathcal{L}_l = \cup_{|\mathcal{I}_\sigma^{\text{in}}|=l} \{\mathcal{O}_\sigma\}$ . Layer  $\mathcal{L}_0 = \{\mathcal{O}^-\}$  is the negative extremal orthant, and  $\mathcal{L}_n = \{\mathcal{O}^+\}$  is the positive extremal orthant. The  $2^n - 2$  transitional orthants form the intermediate layers  $l \in \{1, \dots, n-1\}$ , with each layer containing exactly  $\binom{n}{l}$  distinct orthants.*

*For any two distinct orthants  $\mathcal{O}_{\sigma_a}, \mathcal{O}_{\sigma_b} \in \mathcal{L}_l$  whose sign vectors  $\sigma_a$  and  $\sigma_b$  differ by exactly two indices, their shared boundary is strictly an  $(n-2)$ -dimensional strata. This exclusive intersection constitutes a reciprocal hinge, acting as an orthant hinge simultaneously for both  $\mathcal{O}_{\sigma_a}$  and  $\mathcal{O}_{\sigma_b}$ .*

**Theorem 8** (Global Fiber Capture by Stratified Layers). *For an  $n$ -dimensional kinetic space  $\mathcal{V}$ , any single complete layer  $\mathcal{L}_l$  acts as a complete transverse section to the fiber flow, sufficient to intersect the fibers  $f^{-1}(w)$  for all  $w \in \mathcal{W}$ . The task-space pre-images of the  $\binom{n}{l}$  orthants within a single layer  $\mathcal{L}_l$  possess strictly disjoint interiors—separated by the tangent boundary fibers intersecting the reciprocal hinges—and their union completely partitions the global set of achievable tasks  $w \in \mathcal{W}$ .*

*Proof.* Every continuous reconfiguration fiber originating from  $\mathcal{O}^-$  (layer  $\mathcal{L}_0$ ) and terminating at  $\mathcal{O}^+$  (layer  $\mathcal{L}_n$ ) must strictly and monotonically accumulate entry coordinates, because each  $x_k(\lambda)$  changes sign exactly once. Therefore, every fiber traversing the full kinetic sequence must intersect exactly one orthant in layer  $\mathcal{L}_1$ , one in  $\mathcal{L}_2$ , up through  $\mathcal{L}_{n-1}$ , unless it geometrically intersects a reciprocal hinge. Because fibers intersecting reciprocal hinges are purely tangent (Theorem 6) and define the exact geometric boundaries between the disjoint orthant interiors, the union of the closures of the  $\binom{n}{l}$  orthants in any single layer  $\mathcal{L}_l$  forms a contiguous, complete transverse net. Consequently, the task-space pre-images of the orthants in  $\mathcal{L}_l$  seamlessly piece together to form the entire task space  $\mathcal{W}$ .  $\square$

**Proposition 5** (Combinatorics of Reciprocal Hinges). *The exact number of unique reciprocal hinges contained within a specific orthant layer  $\mathcal{L}_l$  is given by:*

$$N_{\mathcal{H}}(l) = \frac{1}{2} \binom{n}{l} l(n-l) = \binom{n}{2} \binom{n-2}{l-1}. \quad (26)$$

*Proof.* The reciprocal hinges geometrically glue together adjacent orthants within the same layer  $\mathcal{L}_l$ . To transition between two adjacent orthants while remaining strictly within  $\mathcal{L}_l$  (maintaining exactly  $l$  coordinates of a given sign signature), exactly two coordinates must simultaneously vanish and swap signs: one from the  $l$  variables of the given sign signature, and one from the  $n-l$  variables of the opposite signature. Therefore,

from the perspective of any single orthant in  $\mathcal{L}_l$ , there are exactly  $l(n-l)$  possible pairs of coordinates that can form an intra-layer reciprocal hinge.

Summing these possible hinges across all  $\binom{n}{l}$  orthants in the layer counts each hinge twice, because every intra-layer reciprocal hinge is a boundary shared by exactly two adjacent orthants. Dividing by two yields the exact total  $N_{\mathcal{H}}(l)$  in (26).  $\square$

Because the binomial coefficient  $\binom{n-2}{l-1}$  is maximized at the central values of  $l$ , Proposition 5 proves analytically that the deepest transitional layers (centered around  $l \approx n/2$ ) contain the maximum number of reciprocal hinges and, consequently, the highest density of kinematic singularities.

## B. Global Sections in Transitional Layers

The establishment of transitional layers  $\mathcal{L}_l$  provides the exact topological framework required to synthesize the local orthogonal manifolds of each orthant into a global structure. As proven in Theorem 8, the orthants within a single layer  $\mathcal{L}_l$  collectively capture the entire transversal flow of the reconfiguration fibers, with their boundaries contiguous at the reciprocal hinges.

Recall that within any single transitional orthant  $\mathcal{O}_\sigma$ , the orthogonal manifold  $\mathcal{M}_{C,\sigma}$  defined by the level set of the potential function  $\Phi_\sigma(v) = C$  acts as a complete transversal barrier to the local fiber flow within that orthant, anchored at the hinges for any  $C \in \mathbb{R}$ . This localized property scales globally when constrained to a specific layer.

**Definition 8** (Global Orthogonal Section). *For a given transitional layer  $\mathcal{L}_l$  and a fixed potential constant  $C \in \mathbb{R}$ , we define the global orthogonal section  $\mathcal{M}_C^{(l)}$  as the union of the closures of the localized orthogonal manifolds residing in each orthant of that layer:*

$$\mathcal{M}_C^{(l)} = \bigcup_{\sigma \in \mathcal{L}_l} \bar{\mathcal{M}}_{C,\sigma}. \quad (27)$$

*Topologically,  $\mathcal{M}_C^{(l)}$  resembles a multi-petaled structure, where each localized manifold  $\mathcal{M}_{C,\sigma}$  serves as a petal. Because the orthants in  $\mathcal{L}_l$  are structurally glued at their reciprocal hinges, and because the logarithmic potential  $\Phi_\sigma(v) \rightarrow C$  remains consistent at these boundaries, the individual petals are continuously joined at the  $(n-2)$ -dimensional reciprocal hinges.*

Because the layer  $\mathcal{L}_l$  completely partitions the achievable task space  $\mathcal{W}$ , and each petal  $\mathcal{M}_{C,\sigma}$  strictly transverses the fibers of its respective orthant, the orthogonal section  $\mathcal{M}_C^{(l)}$  constitutes a complete, global orthogonal section of the entire task-space fiber bundle. Every fiber intersects  $\mathcal{M}_C^{(l)}$  orthogonally and exactly once.

**Theorem 9** ( $C^1$  Smoothness of Global Sections). *For any transitional layer  $\mathcal{L}_l$  ( $l \in \{1, \dots, n-1\}$ ) and any constant  $C \in \mathbb{R}$ , the global orthogonal section  $\mathcal{M}_C^{(l)}$  is a  $C^1$  smooth differential manifold across its interior. Specifically, at any*

reciprocal hinge joining two adjacent orthants  $\mathcal{O}_A, \mathcal{O}_B \in \mathcal{L}_l$ , the tangent hyperplanes of the respective local manifolds  $\mathcal{M}_{C,A}$  and  $\mathcal{M}_{C,B}$  continuously align.

*Proof.* Let  $p$  be a point strictly residing on a reciprocal hinge that forms the shared boundary between two adjacent orthants  $\mathcal{O}_A$  and  $\mathcal{O}_B$  within  $\mathcal{L}_l$ . By Definition 7,  $\mathcal{O}_A$  and  $\mathcal{O}_B$  differ in exactly two coordinate signs. Let these indices be  $i$  and  $j$ , such that  $\sigma_i^B = -\sigma_i^A$  and  $\sigma_j^B = -\sigma_j^A$ .

Because  $p$  lies on this reciprocal hinge, the kinetic coordinates approach zero exactly at these indices:  $v_i \rightarrow 0$  and  $v_j \rightarrow 0$ , while all other spatial coordinates  $v_k$  (for  $k \neq i, j$ ) remain strictly non-zero and finite. To simplify notation, let  $\alpha = \sigma_i^A b_i^A$  and  $\beta = \sigma_j^A b_j^A$ . Because one index represents an entry face and the other an exit face,  $\alpha$  and  $\beta$  possess opposite signs. Without loss of generality, assume  $\alpha > 0$  and  $\beta < 0$ , and define  $\gamma = -\beta > 0$ .

Consider the normal vector to the petal  $\mathcal{M}_{C,A}$  within the interior of  $\mathcal{O}_A$ , given by the gradient of the potential function:

$$\nabla\Phi_A(v) = \left[ \dots, \frac{\alpha}{v_i}, \dots, \frac{-\gamma}{v_j}, \dots \right]^T. \quad (28)$$

As  $v \rightarrow p$ , the components  $i$  and  $j$  diverge to infinity, while all other components remain finite. Consequently, the unit normal vector  $\hat{n}_A = \frac{\nabla\Phi_A}{\|\nabla\Phi_A\|}$  collapses strictly into the two-dimensional  $v_i - v_j$  plane. The geometric orientation of this normal vector within that plane is defined by the ratio of its components:

$$R_A = \frac{(\nabla\Phi_A)_j}{(\nabla\Phi_A)_i} = -\frac{\gamma}{\alpha} \left( \frac{v_i}{v_j} \right). \quad (29)$$

The asymptotic behavior of the ratio  $(v_i/v_j)$  is governed by the level set constraint  $\Phi_A(v) = C$ . Let  $S(p)$  be the finite sum of the remaining potential terms evaluated at  $p$ . The constraint requires  $\alpha \ln(v_i) - \gamma \ln(v_j) + S(p) = C$ . Solving for  $v_i$  yields  $v_i = v_j^{\gamma/\alpha} e^{(C-S(p))/\alpha}$ . Substituting this into the ratio  $R_A$  gives:

$$R_A = -\frac{\gamma}{\alpha} v_j^{(\frac{\gamma}{\alpha}-1)} e^{\frac{C-S(p)}{\alpha}}. \quad (30)$$

The limit of  $R_A$  as  $v_j \rightarrow 0$  depends strictly on the system parameters  $\alpha$  and  $\gamma$ :

- *Asymmetric Case I* ( $\gamma > \alpha$ ): The exponent  $(\gamma/\alpha - 1)$  is positive. As  $v_j \rightarrow 0$ ,  $R_A \rightarrow 0$ . The normal vector fully aligns with the  $v_j$  axis, independent of  $C$ .
- *Asymmetric Case II* ( $\gamma < \alpha$ ): The exponent is negative. As  $v_j \rightarrow 0$ ,  $R_A \rightarrow -\infty$ . The normal vector fully aligns with the  $v_i$  axis, independent of  $C$ .
- *Symmetric Case* ( $\gamma = \alpha$ ): The exponent is zero. As  $v_j \rightarrow 0$ ,  $R_A \rightarrow -e^{(C-S(p))/\alpha}$ . The normal vector converges to a specific diagonal angle dictated by the level set constant  $C$ .

Now consider the adjacent petal  $\mathcal{M}_{C,B}$  within  $\mathcal{O}_B$ . Its potential gradient components for  $i$  and  $j$  negate exactly:  $(\nabla\Phi_B)_i = -\alpha/v_i$  and  $(\nabla\Phi_B)_j = \gamma/v_j$ . The planar ratio evaluates to  $R_B = \frac{\gamma/v_j}{-\alpha/v_i} \equiv R_A$ . Because the finite remainder  $S(p)$  relies only on the  $n - 2$  coordinates whose signs are

identical across both orthants,  $S(p)$  is invariant. Because the level-set constant  $C$  is identically enforced, the limit of  $R_B$  evaluates to the exact same geometrically parallel normal direction as  $R_A$  across all three parametric cases.

Because the dominant, infinite components of  $\nabla\Phi_B$  are the exact algebraic negations of  $\nabla\Phi_A$ , and their planar ratios match perfectly, their unit normal vectors in the limit satisfy  $\lim_{v \rightarrow p} \hat{n}_B(v) = -\lim_{v \rightarrow p} \hat{n}_A(v)$ . A unit normal vector and its exact negation define the identical unoriented one-dimensional normal space. Their orthogonal complements—the tangent hyperplanes  $T_p\mathcal{M}_{C,A}$  and  $T_p\mathcal{M}_{C,B}$ —are therefore geometrically identical. Thus, the global section  $\mathcal{M}_C^{(l)}$  connects smoothly at the reciprocal hinges, guaranteeing  $C^1$  continuity.  $\square$

**Remark 5** (Topological Necessity of a Global Constant  $C$ ). *The proof of Theorem 9 reveals a geometric nuance: in the asymmetric cases ( $|\alpha| \neq |\beta|$ ), the explosive divergence of the gradient forces the tangent plane to align with the bounding axes independently of the level set constant  $C$ . Geometrically, this implies that one could artificially construct a piecewise manifold by gluing a local petal  $\mathcal{M}_{C_A,A}$  to a neighboring petal  $\mathcal{M}_{C_B,B}$  (where  $C_A \neq C_B$ ), and in asymmetric conditions, the resulting surface might still retain  $C^1$  smoothness.*

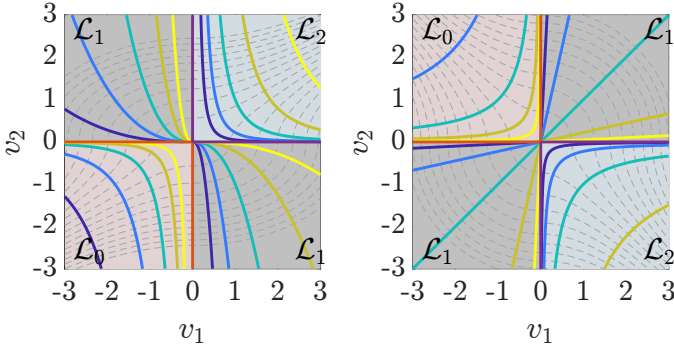
However, enforcing a uniform global constant  $C$  across the entire layer  $\mathcal{L}_l$  is topologically mandatory. First, for parametric robustness, as demonstrated in the symmetric case ( $|\alpha| = |\beta|$ ), if the kinetic parameters of the crossing variables are balanced, the tangent angle becomes strictly reliant on  $C$ . Gluing disparate  $C$  values in this regime would result in a sharp transversal kink, destroying  $C^1$  continuity. Second, the global manifold  $\mathcal{M}_C^{(l)}$  represents an isopotential barrier to the transversal fiber flow. Enforcing  $C_A = C_B = C$  preserves the continuous physical dynamics of the configuration space. Sweeping the single constant  $C \in (-\infty, \infty)$  ensures that the global manifolds cleanly foliate the entire transitional layer  $\mathcal{L}_l$ , creating a continuous, non-intersecting (despite being tangent at the reciprocal hinges), one-to-one mapping of the global task space.

A visual demonstration of some of the main concepts introduced in this section is shown in Figs. 3, 4, and 5. While those figures refer unavoidably to the low dimension cases  $n = 2$  and  $n = 3$ , they are instrumental to build an intuition for the geometry developed so far which is valid in any higher dimension  $n \in \mathbb{N}$ .

## VI. SUMMARY: GLOBAL ORTHOGONAL FOLIATION OF THE KINETIC SPACE

The geometric structure detailed in the preceding analysis can be characterized in the framework of differential geometry as a global orthogonal foliation, formed by exact orthogonal sections of a fiber bundle. We recap and summarize these theoretical results into a list of geometric properties.

Let  $f : \mathcal{V} \rightarrow \mathcal{W}$  denote the nonlinear signed-quadratic mapping (1) from the punctured kinetic space  $\mathcal{V} \subseteq \mathbb{R}^n \setminus \{0\}$  to



(a) Asymmetr. Case ( $|\alpha| \neq |\beta|$ ). (b) Balanced Case ( $|\alpha| = |\beta|$ ).

Fig. 3: Global orthogonal sections and layer partitioning in a low dimension  $n = 2$  kinetic space. The phase space is stratified into distinct topological layers ( $\mathcal{L}_0, \mathcal{L}_1, \mathcal{L}_2$ ), indicated by the background shading. In  $\mathcal{L}_1$  the fibers (dashed gray) flow strictly from the entry portals (orange) to the exit portals (purple). The global sections  $\mathcal{M}_C^{(1)}$  act as complete orthogonal transversal barriers, seamlessly gluing the local orthant petals across the reciprocal hinge (the point  $(0, 0)$  for  $n = 2$ ) to form a continuous,  $C^1$  smooth mapping of the task space.

the task space  $\mathcal{W} \cong \mathbb{R}^m$ . The preimages of the task variables define a family of one-dimensional fibers:

$$f^{-1}(w) = \{v \in \mathcal{V} \mid f(v) = w\}. \quad (31)$$

The analysis establishes the existence of a family of  $m$ -dimensional orthogonal manifolds, denoted  $\mathcal{M}_\kappa$ , where  $\kappa$  uniquely identifies each manifold being  $\kappa = (l, C) \in \mathcal{I}$ , where  $\mathcal{I} = \{0, \dots, n\} \times \mathbb{R}$  and  $l$  denotes the manifold's strict confinement to a specific topological layer ( $\mathcal{M}_\kappa \subset \mathcal{L}_l$ ) and  $C$  represents its constant potential value ( $\Phi(v) = C$ ). The topological and geometric properties of these manifolds depend strictly on their layer confinement:

- 1) *Topological Regularity of Extremal Sections:* For orthogonal manifolds constrained entirely within the interior of the extremal layers ( $l \in \{0, n\}$ , such that  $\mathcal{M}_\kappa \subset \mathcal{L}_0^\circ \cup \mathcal{L}_n^\circ$ ), the orthogonal manifolds never intersect the coordinate axes nor the origin. Consequently, the restriction of the map,  $f|_{\mathcal{M}_\kappa} : \mathcal{M}_\kappa \rightarrow \mathcal{W}$ , is a global diffeomorphism. These sections act as exact, globally smooth orthogonal cross-sections of the fiber bundle.
- 2) *Singular Boundaries in Transitional Sections:* For orthogonal manifolds spanning the transitional layers ( $l \in \{1, \dots, n-1\}$ ), the sections asymptotically converge toward the origin. Because the origin acts as a topological center but is strictly excluded from  $\mathcal{V}$ , there is no state  $v \in \mathcal{M}_\kappa$  that maps to the origin of  $\mathcal{W}$ . Therefore, the mapping must be restricted to the punctured task space  $\mathcal{W} \setminus \{0\}$ . Furthermore, the mapping is structurally partitioned by intersections with a singular set composed of hinges, defined as  $\mathcal{H}_\kappa = \{v \in \mathcal{M}_\kappa \mid \exists i \neq j \text{ s.t. } |v_i| + |v_j| = 0\}$ . These hinges act as lower-dimensional boundaries that connect the disjoint orthant-specific segments (the ‘petals’) of the full manifold. Consequently:

- Topologically,  $f|_{\mathcal{M}_\kappa}$  establishes a global homeomorphism between the transitional section  $\mathcal{M}_\kappa$  and the punctured task space  $\mathcal{W} \setminus \{0\}$ .
- Differentially, at the hinges  $v \in \mathcal{H}_\kappa$ , the Jacobian loses full rank, meaning the mapping fails to be a diffeomorphism at these boundaries.
- Restricted strictly to the interior of the orthants, the mapping is locally smooth. The manifold domain excluding the hinges,  $\mathcal{M}_\kappa \setminus \mathcal{H}_\kappa$ , is strictly diffeomorphic to  $\mathcal{W} \setminus f(\mathcal{H}_\kappa)$ .
- As established in Proposition 5, the closer the transitional layers are to the middle ( $l \approx n/2$ ), the larger the number of hinges. This progressively excises more singular boundaries from the valid diffeomorphic mapping to the task space, and causes the partition of  $\mathcal{W}$  into more and smaller images of the orthants of  $\mathcal{L}_l$ .

- 3) *Orthogonal Transversality:* At any non-singular state  $v$  ( $v \in \mathcal{M}_\kappa$  for extremal sections, and  $v \in \mathcal{M}_\kappa \setminus \mathcal{H}_\kappa$  for transitional sections), the tangent space of the manifold is strictly orthogonal to the tangent space of the intersecting fiber. That is,  $T_v \mathcal{M}_\kappa \perp T_v \mathcal{F}_{f(v)}$ , perfectly satisfying the condition of an orthogonal distribution.
- 4) *Kinetic Space Foliation:* The continuous family of manifolds partitions the domain  $\mathcal{V}$ . Every valid kinetic state  $v \in \mathcal{V}$  belongs to exactly one manifold  $\mathcal{M}_\kappa$ . Therefore, the manifolds constitute a complete foliation of the available kinetic space:

$$\mathcal{V} = \bigsqcup_{\kappa \in \mathcal{I}} \mathcal{M}_\kappa. \quad (32)$$

## VII. STATIC CONTROL ALLOCATION: ORTHOGONAL SECTIONS VERSUS PSEUDO-LINEAR INVERSES

In this section, we compare different strategies for redundancy resolution in light of the global geometry of the fibers and the orthogonal manifolds established in the preceding analysis. We begin by recalling the concept of a static allocation mapping.

### A. Recap on Static Allocators

When a mapping  $f$  projects a higher-dimensional space onto a lower-dimensional one, it induces the structure of a fiber bundle. A subset of  $\mathcal{V}$  that intersects every valid fiber exactly once and maps diffeomorphically to the punctured task space is defined as a *global section* (or cross-section).

**Definition 9** (Static Allocator and Global Section). *In the context of control allocation, finding a global section equates to defining a static allocator, which constitutes a global right-inverse of the map  $f$ . The image of this right-inverse is the manifold representing the section itself. Because any kinetic state  $v \in \mathcal{V}$  must lie on a fiber parameterized by  $\lambda$  in the transformed space, any static allocator  $h : \mathcal{W} \rightarrow \mathcal{V}$  satisfying  $f(h(w)) = w$  is uniquely defined by a continuous scalar field  $\Lambda : \mathcal{W} \rightarrow \mathbb{R}$ . This field assigns a specific fiber parameter to each task  $w$ , defining the global right-inverse:*

$$h(w) = g^{-1}(A^+ w + \Lambda(w) b^A). \quad (33)$$

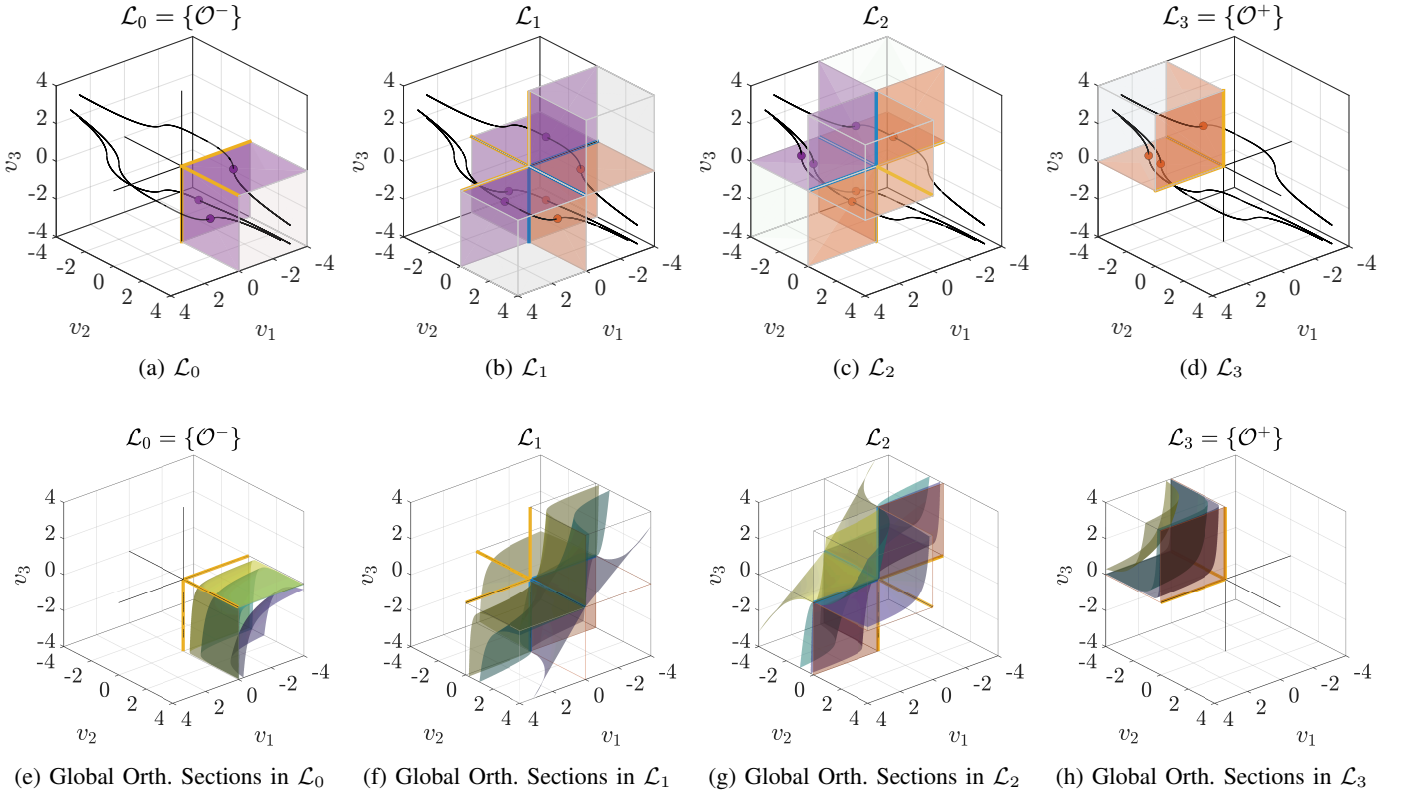


Fig. 4: Global stratification and orthogonal sections of a 3D kinetic space ( $n = 3$ ). (Top Row) The sequential layer partition  $\mathcal{L}_0 \rightarrow \mathcal{L}_3$ . Exit portals are indicated in purple and entry portals in orange; folds are represented by blue semi-axes and hinges by gold semi-axes. The extremal layers are bounded exclusively by either exit portals (for the negative extremal orthant  $\mathcal{L}_0 = \{\mathcal{O}^-\}$ ) or entry portals (for the positive extremal orthant  $\mathcal{L}_3 = \{\mathcal{O}^+\}$ ). In both extremal cases, the bounding axes consist entirely of folds. The transitional layers  $\mathcal{L}_1$  and  $\mathcal{L}_2$  contain intermediate orthants geometrically glued by reciprocal hinges. The structural designations of the folds and hinges invert when transitioning from  $\mathcal{L}_1$  to  $\mathcal{L}_2$ . Representative reconfiguration fibers (black curves) strictly traverse this sequence. Intersections with the spatial boundaries are rigidly categorized: fibers pierce entry portals (orange faces) at entry nodes (orange markers) and leave via exit portals (purple faces) at exit nodes (purple markers). (Bottom Row) The corresponding global orthogonal sections  $\mathcal{M}_C^{(l)}$  foliating each layer, evaluated at level-set constants  $C \in \{-3, 0, 3\}$  (translucent colored surfaces). Within the transitional layers  $\mathcal{L}_1$  and  $\mathcal{L}_2$ , the localized orthogonal sections converge continuously at the reciprocal portals and bend toward the folds, which subsequently evolve into the hinges of the next layer. Across these transitional layers, the component orthogonal manifolds are structurally glued at the hinges to maintain  $C^1$  smoothness, establishing the global section as a complete, smooth transversal barrier to the fiber flow.

where  $g$  has been introduced in Def. 2.

The choice of the function  $\Lambda(w)$  strictly dictates the geometry of the resulting allocation manifold  $\mathcal{M}_\Lambda = \{h(w) \mid w \in \mathcal{W} \setminus \{0\}\}$ . We categorize these allocators into distinct geometric families.

**Definition 10** (Allocator Families). *Based on the properties of the scalar field  $\Lambda(w)$ , static allocators are categorized as follows:*

1) **Orthogonal Allocators** ( $\Lambda_{orth}$ ): *As established, the exact leaves of the orthogonal foliation are parameterized by the index tuple  $\kappa = (l, C) \in \mathcal{I}$ . To ensure the system state remains confined to a specific chosen orthogonal manifold  $\mathcal{M}_\kappa$ , its corresponding target layer  $\mathcal{L}_l$  and constant potential  $C$  must be strictly maintained.*

*To achieve this, the orthogonal allocator  $\Lambda_{orth}(w; \kappa)$  is implicitly defined as the unique, continuous root that satisfies*

*the potential constraint for the resulting kinetic state:*

$$\Phi(v) = C, \quad \text{where } v = g^{-1}(A^+w + \Lambda_{orth}b^A) \in \mathcal{L}_l. \quad (34)$$

*As the task  $w$  varies, the scalar  $\Lambda_{orth}(w; \kappa)$  adapts nonlinearly to isolate this unique manifold  $\mathcal{M}_\kappa$ , preserving strict orthogonal transversality with the fibers.*

- 2) **Warped Allocators** ( $\Lambda(w)$ ): *Any arbitrary smooth function  $\Lambda(w)$  that does not satisfy the potential constraint (34) defines a warped allocator. The resulting manifold  $\mathcal{M}_\Lambda$  remains diffeomorphic to the task space and intersects every fiber exactly once, but it loses the geometric property of orthogonal transversality, representing a warped right-inverse.*
- 3) **Constant- $\lambda$  Allocators** ( $\Lambda(w) = \lambda_0$ ): *The simplest example of a warped allocator fixes the fiber parameter to a global constant  $\lambda_0$  regardless of the task. The resulting manifold  $\mathcal{M}_{\lambda_0}$  forms a flat affine subspace in the transformed space  $\mathcal{X}$ . However, due to the nonlinear mapping  $g^{-1}$ , the*

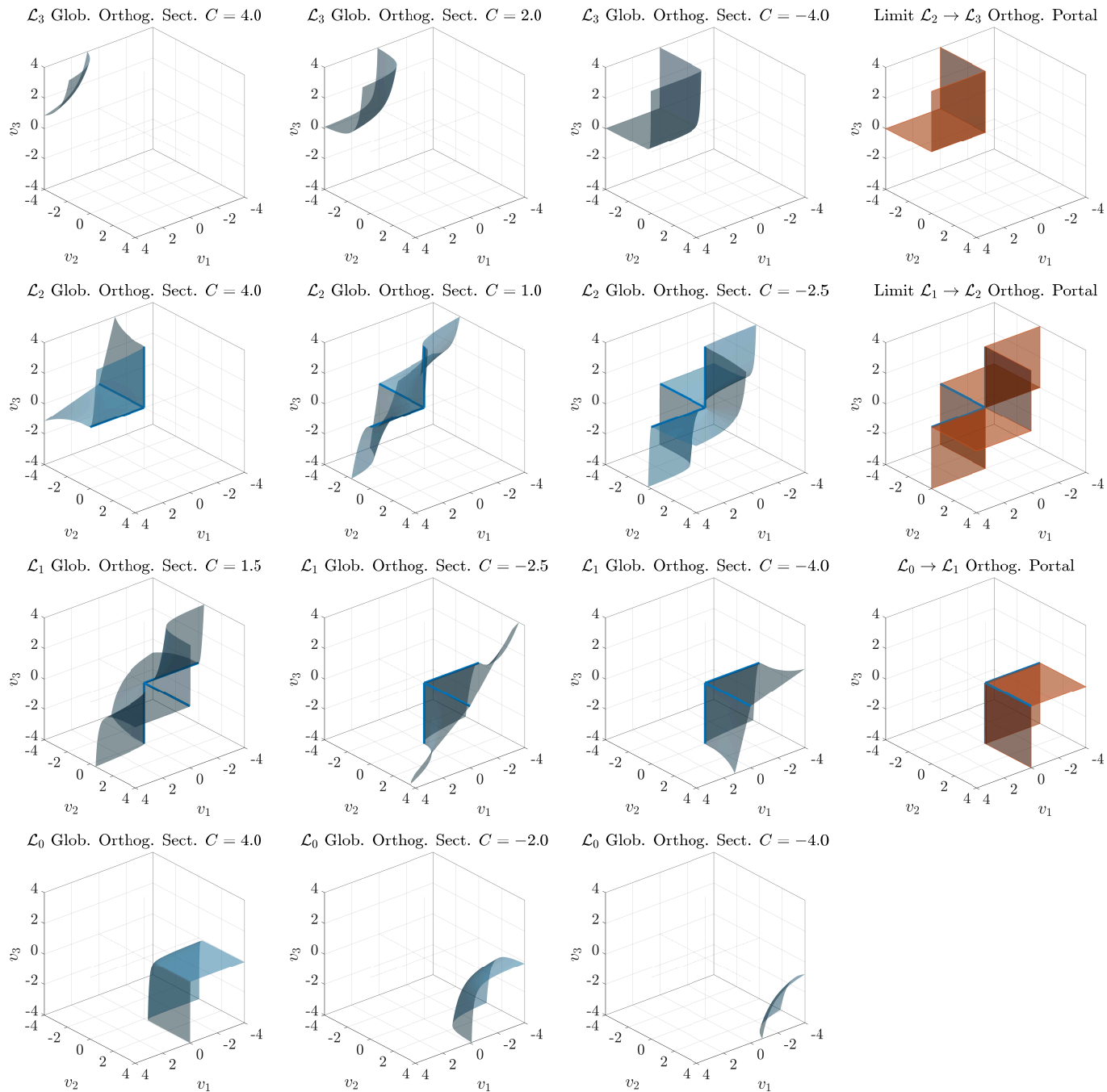


Fig. 5: Sequential progression of the global orthogonal sections already displayed in Fig. 4 but this time displayed separately for better visualization. Displayed in reverse order from the positive external orthant ( $\mathcal{L}_3$ , top left) back to the negative external orthant ( $\mathcal{L}_0$ , bottom row). Passing through all the intermediate layers and the portals between them.

projection of this subspace into the kinetic space  $\mathcal{V}$  yields a skewed, non-orthogonal section that warps across the orthants.

Because the orthogonal foliation completely partitions the valid kinetic space, any arbitrary operating point  $v \in \mathcal{V}$  belongs to exactly one orthogonal manifold  $\mathcal{M}_\kappa$ . Thus, it represents the unique solution to the orthogonal allocator  $\Lambda_{orth}(\cdot; \kappa)$  evaluated at  $w = f(v)$  for the specific layer  $\mathcal{L}_l$  containing  $v$  and the potential  $C = \Phi(v)$ .

**Remark 6** (Motivation for Warped Allocators). *The orthogonal allocators  $\Lambda_{orth}(w; \kappa)$  provide a geometrically elegant baseline that strictly respects the potential field of the fibers. However, practical control applications sometimes demand a deliberate departure from strict orthogonality. Purposefully shaping the scalar field  $\Lambda(w)$  offers distinct operational advantages over strict orthogonal resolution:*

- **Task-Specific Sculpting:** *The strict level sets of the orthogonal foliation rigidly lock how the kinetic state  $v$  distributes across the orthants for a given task. By shaping  $\Lambda(w)$ , the allocation manifold  $\mathcal{M}_\Lambda$  can be explicitly sculpted. This allows specific regions of  $\mathcal{W}$  to be mapped to preferred kinetic orthants, embedding hardware constraints, asymmetrical saturation limits, or preferred actuator configurations directly into the static right-inverse.*
- **Dynamic Response Tuning:** *The local geometry of the chosen manifold dictates the system's differential kinematics. Specifically, the tangent space of  $\mathcal{M}_\Lambda$  governs the differential mapping  $\dot{v} = \nabla h(w)\dot{w}$ . By systematically perturbing  $\Lambda(w)$  away from the orthogonal baseline, the gradient is explicitly tuned offline. This enables custom, state-dependent differential behavior without the computational overhead of calculating a local weighted pseudo-inverse at every control step.*

In the remainder of this section, we compare static allocation based on the geometric orthogonal foliation introduced herein—specifically utilizing the transitional and extremal orthogonal manifolds—against the classical pseudo-linear allocator widely adopted in the literature.

### B. Pseudo-Linear Allocators versus Global Orthogonal Sections

A standard approach to redundancy resolution for maps like  $f(v)$  relies on the fact that they can be transformed into linear maps  $(f \circ g^{-1})(x) = Ax$  via the nonlinear homeomorphism  $g : v \mapsto x \triangleq v \odot |v|$ . We refer to allocation in the transformed space as pseudo-linear mapping, because any solution must eventually be mapped back to the native kinetic state via the nonlinear inverse  $g^{-1}$ .

**Definition 11** (Pseudo-Linear Allocator). *A pseudo-linear allocator is defined by an  $m$ -dimensional affine subspace  $\mathcal{S}_x \subset \mathbb{R}^n$  in the auxiliary transformed space that satisfies the direct sum condition with the null-space of the allocation matrix:*

$$\mathcal{S}_x \oplus \ker(A) = \mathbb{R}^n. \quad (35)$$

This ensures the restriction  $A|_{\mathcal{S}_x} : \mathcal{S}_x \rightarrow \mathcal{W}$  is a linear isomorphism. The corresponding allocation manifold in the kinetic space  $\mathcal{V}$  is obtained via the inverse mapping  $v = g^{-1}(x) = \text{sign}(x) \odot \sqrt{|x|}$ , yielding  $\mathcal{M}_{PL} = g^{-1}(\mathcal{S}_x)$ .

While  $\mathcal{M}_{PL}$  constitutes a valid global section (diffeomorphic to  $\mathcal{W}$  almost everywhere), it suffers from two critical geometric and kinematic drawbacks:

- 1) **Loss of Orthogonality:** Even if  $\mathcal{S}_x$  is strictly orthogonal to the fibers in the transformed space (e.g., utilizing the Moore-Penrose pseudo-inverse  $x_{PL}(w) = A^+w$ ), the mapping  $g^{-1}$  is non-conformal. The Jacobian  $J_{g^{-1}}(x) = \text{diag}\left(\frac{1}{2\sqrt{|x_i|}}\right)$  locally skews the tangent space, meaning the resulting manifold  $\mathcal{M}_{PL}$  loses orthogonal transversality with the fibers in the native kinetic space  $\mathcal{V}$ .
- 2) **Kinetic Singularities at Orthant Boundary Crossings:** The pseudo-linear mapping  $x = A^+w$  defines an  $m$ -dimensional linear subspace  $\mathcal{S}_x$  passing through the origin. Consequently, this subspace intrinsically intersects the  $n$  coordinate hyperplanes ( $x_i = 0$ ), forming  $(m - 1)$ -dimensional singularity sets within the manifold. These singular sets exhibit mutual intersections, all of which converge at the origin.

Any continuous trajectory within  $\mathcal{S}_x$  that transitions between different orthants must inevitably cross these hyperplanes. The required evolution of the kinetic state during such a crossing is governed by the chain rule:

$$\dot{v}_i = \frac{\dot{x}_i}{2\sqrt{|x_i|}}. \quad (36)$$

As  $x_i \rightarrow 0$ , the required actuator rate diverges to infinity unless the task trajectory coincidentally ensures  $\dot{x}_i \rightarrow 0$ . Physically, if  $v$  represents a rotor spin rate, this divergence corresponds to an infinite angular acceleration, fundamentally violating the unavoidable constraints of limited motor torque. Therefore, any static pseudo-linear allocator intrinsically imposes unavoidable kinetic singularities at the exact core of the workspace.

To demonstrate why the singularities caused by (36) are unavoidably triggered by pseudo-linear strategies, we analyze how these allocators interact with the orthants.

**Proposition 6** (Extremal Exclusion of the Pseudo-Inverse). *The static allocator defined by the Moore-Penrose pseudo-inverse,  $x_{PL}(w) = A^+w$ , is strictly confined to the transitional orthants and cannot intersect the extremal orthants  $\mathcal{O}^+$  or  $\mathcal{O}^-$ .*

*Proof.* By definition,  $x_{PL} \in \ker(A)^\perp$ , requiring the inner product  $(b^A)^T x_{PL} = \sum_{i=1}^n b_i^A x_{PL,i} = 0$ . However, any point  $x \in \mathcal{O}^+ \cup \mathcal{O}^-$  satisfies  $\text{sign}(x_i) = \pm \text{sign}(b_i^A)$  for all  $i$ . This implies the terms  $b_i^A x_i$  are either all strictly positive or all strictly negative, yielding  $\sum_{i=1}^n b_i^A x_i \neq 0$ . This contradicts the orthogonality condition, proving the exclusion.  $\square$

While the pseudo-linear subspace  $\mathcal{S}_x$  is strictly excluded from the extremal orthants—rendering it inherently distinct from any extremal orthogonal section  $\mathcal{M}_{l,C}$  with  $C \in \mathbb{R}$  and  $l \in \{0, n\}$ —its geometric behavior across the remaining space reveals fundamental structural differences also when compared to the orthogonal sections within the transitional orthants ( $l \in \{1, \dots, n-1\}$ ). To form a valid global section, an allocation manifold is not required to intersect all available transitional orthants. The theory developed in Sec. V has shown that confining the manifold to the  $\binom{n}{l}$  orthants of a single intermediate layer  $\mathcal{L}_l$  is sufficient to map the entire task space  $\mathcal{W}$ . In stark contrast, the pseudo-inverse distributes its mapping across the entirety of the transitional space.

**Proposition 7** (Global Transitional Intersection). *The  $m$ -dimensional pseudo-linear subspace  $\mathcal{S}_x = \text{Im}(A^T)$  strictly intersects all  $2^n - 2$  transitional orthants.*

*Proof.* Let  $\mathcal{O}_\sigma$  be a transitional orthant characterized by a sign vector  $\sigma \in \{-1, 1\}^n$ . Because  $\mathcal{O}_\sigma$  is transitional,  $\sigma \neq \pm \text{sign}(b^A)$ . Therefore, the index set  $\{1, \dots, n\}$  partitions into two non-empty subsets:  $\mathcal{I}^+ = \{i \mid \sigma_i = \text{sign}(b_i^A)\}$  and  $\mathcal{I}^- = \{i \mid \sigma_i = -\text{sign}(b_i^A)\}$ . For any  $x \in \mathcal{O}_\sigma$ , the inner product with  $b^A$  expands as:

$$(b^A)^T x = \sum_{i \in \mathcal{I}^+} |b_i^A| |x_i| - \sum_{i \in \mathcal{I}^-} |b_i^A| |x_i|. \quad (37)$$

Because both  $\mathcal{I}^+$  and  $\mathcal{I}^-$  are non-empty and  $|b_i^A| > 0$  for all  $i$  (Assumption 2), there always exists a choice of strictly positive magnitudes  $|x_i| > 0$  such that the two sums are equal, satisfying  $(b^A)^T x = 0$ . Thus, there exists a valid allocation  $x \in \mathcal{S}_x \cap \mathcal{O}_\sigma$  for every transitional orthant.  $\square$

This geometric property highlights a structural trade-off regarding the topological strata where orthant transitions occur. For the pseudo-inverse allocator  $\mathcal{S}_x$ , transitioning between orthants typically features exactly one vanishing coordinate ( $x_i = 0$ ), crossing  $(n-1)$ -dimensional boundary hyperplanes. Conversely, orthogonal sections constrained to a specific layer  $\mathcal{L}_l$  piece together adjacent orthants at reciprocal hinges, where two coordinates vanish simultaneously ( $x_i = x_j = 0$ ), corresponding to lower-dimensional  $(n-2)$  strata.

Traversing an  $(n-1)$ -dimensional stratum imposes an infinite time derivative on a single actuator (remember (36)). Crossing an  $(n-2)$ -dimensional stratum forces the kinematic Jacobian to strictly lose rank, representing a momentary loss of geometric direction in the tangent space of  $\mathcal{V}$ , which is a more critical topological discontinuity than a purely temporal singularity. In this specific regard, the pseudo-inverse allocator possesses a slight geometric advantage during boundary crossings when compared to orthogonal allocators in transitional layers.

Nevertheless, both allocation strategies partition the task space  $\mathcal{W}$  into conical subsets, or wedges, representing the pre-image  $h^{-1}(\mathcal{O}_\sigma)$ . Within the interior of these wedges, both methods provide a smooth diffeomorphism. The critical operational distinction lies in the density of this partition:

- *Frequency of Boundary Crossings: Exponential vs Linear*  
Because the pseudo-linear allocator partitions the task space  $\mathcal{W}$  into  $2^n - 2$  distinct wedges, whereas an orthogonal section in layer  $\mathcal{L}_l$  partitions  $\mathcal{W}$  into only  $\binom{n}{l}$  wedges, the pseudo-inverse regions enclose significantly smaller solid angles. Consequently, an arbitrary continuous trajectory in  $\mathcal{W}$  will undergo boundary crossings considerably more frequently under the pseudo-linear mapping. This structural advantage of the orthogonal foliation is exponentially magnified for layers adjacent to the extremal orthants ( $l = 1$  or  $l = n - 1$ ). In such configurations, the orthogonal manifold partitions the space into merely  $\binom{n}{1} = \binom{n}{n-1} = n$  wedges, yielding an exponential reduction in boundary density compared to the  $2^n$  exponential scaling of the baseline allocator.
- *Expansion of Unidirectional Task Capacity:* For systems restricted to unidirectional actuators, the physically permissible kinetic state is strictly confined to a single orthant. Under the pseudo-linear mapping, the feasible task space is limited to just one wedge out of the exponential  $2^n$  partitions, yielding a highly conservative operational footprint in  $\mathcal{W}$ . Conversely, a transitional orthogonal allocator parameterized by  $\kappa = (l, C)$  partitions  $\mathcal{W}$  into only  $\binom{n}{l}$  regions (i.e.,  $n$ , for  $l = 1$  and  $l = n - 1$ ). Because the total task space is divided among significantly fewer preimages, the solid angle of  $\mathcal{W}$  mapped into the single valid operational orthant is structurally expanded. Therefore, by operating within an appropriately selected transitional layer, the orthogonal allocator inherently captures a substantially larger continuous task-space volume than the restrictive bounds imposed by the pseudo-inverse baseline.

### C. Allocations Based on Extremal Orthogonal Sections

Both pseudo-linear allocators and transitional orthogonal sections require piecing together multiple orthants, inherently forcing the system to navigate boundary singularities when the task trajectory crosses between sectors. To establish a truly global, singularity-free static allocation, the manifold must be entirely contained within a single orthant while still maintaining global surjectivity onto  $\mathcal{W}$ . The extremal orthogonal manifolds uniquely satisfy this topological requirement.

**Theorem 10** (Singularity Avoidance of Extremal Allocators). *Static allocations based on the extremal orthogonal manifolds entirely circumvent the geometric trap of boundary singularity crossings. By strictly occupying the extremal orthants ( $\mathcal{O}^+$  and  $\mathcal{O}^-$ ), from which the pseudo-linear subspace  $\mathcal{S}_x$  is excluded, and remaining strictly asymptotic to the coordinate hyperplanes ( $v_i \neq 0$ ), these allocators provide a global diffeomorphism to the entire unbounded task space  $\mathcal{W}$  while remaining permanently confined to a single orthant. Consequently, they represent a global static allocation strategy that guarantees the avoidance of both geometric rank-loss and infinite-derivative temporal singularities.*

*Proof.* By Theorem 7, an orthogonal manifold  $\mathcal{M}_C$  residing in an extremal orthant ( $\mathcal{O}^+$  or  $\mathcal{O}^-$ ) possesses no hinges

( $\mathcal{H} = \emptyset$ ). Because  $\mathcal{H} = \emptyset$ , the manifold never intersects the  $(n - 2)$ -dimensional boundary strata, thereby strictly avoiding the geometric rank-loss singularities of the Jacobian. Furthermore, for any finite potential constant  $C \in \mathbb{R}$ , the manifold remains strictly asymptotic to the entry portal  $\mathcal{P}_\sigma^{in}$  without ever intersecting the  $(n - 1)$ -dimensional coordinate hyperplanes ( $v_i \neq 0$ ). Thus, the continuous trajectory along the manifold strictly avoids the infinite-derivative temporal singularities defined in (36).

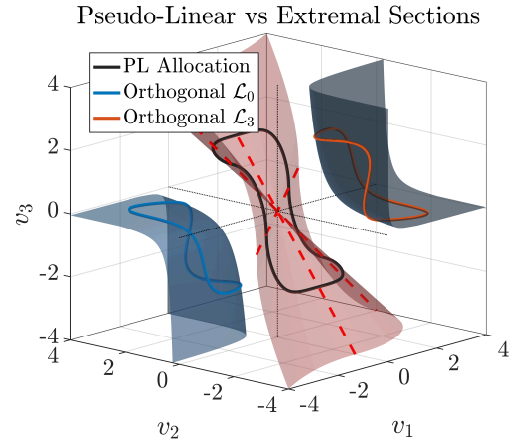
Concurrently, Theorem 3 established that the restriction of the actuation map  $f(v)$  to either extremal orthant is globally surjective onto  $\mathcal{W}$ . Because  $\mathcal{M}_C$  is a continuous, non-intersecting global section that sweeps the extremal orthant, its restriction  $f|_{\mathcal{M}_C} : \mathcal{M}_C \rightarrow \mathcal{W}$  is a global diffeomorphism. Therefore, the extremal allocator maps the entire task space without ever crossing a kinetic boundary. Finally, by Proposition 6, the pseudo-linear subspace  $\mathcal{S}_x$  is excluded from these extremal orthants, proving that this singularity-free global allocation is an exclusive property of the orthogonal (or warped) nonlinear sections.  $\square$

To provide an intuitive visual consolidation of these theoretical properties, Figure 6 illustrates the geometric structures of the respective allocators for a system with  $n = 3$  actuators and an  $m = 2$  dimensional task space. The visualization explicitly highlights the larger spatial fragmentation induced by the classical pseudo-linear allocator compared to allocators based on the orthogonal sections. As derived analytically, the pseudo-linear manifold exhibits intrinsic non-orthogonal warping in the kinetic space  $\mathcal{V}$  and is fractured by  $2^3 - 2 = 6$  boundary intersection lines. Conversely, the orthogonal manifolds in transitional layers have  $\binom{3}{1} = 3$  boundaries, and ones in the extremal layers eliminate boundary crossings entirely, mapping a continuous task-space trajectory via a global diffeomorphism.

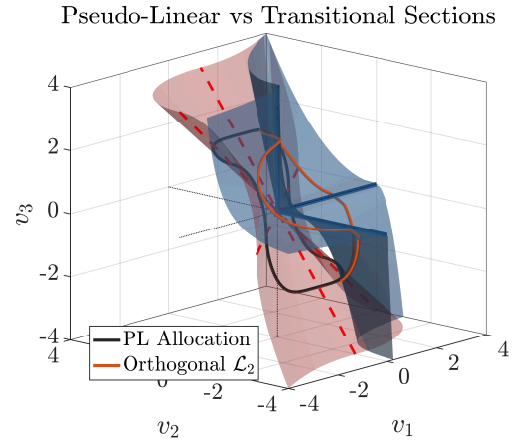
## VIII. DISCUSSION AND CONCLUSION

This work establishes a differential geometric foundation for the control allocation of redundant systems governed by signed-quadratic actuation maps. Rather than relying on classical pseudo-linear algebraic projections or local numerical solvers, this analysis formalizes the native topological structure of the kinetic space (the space of the actuators).

A primary theoretical result is the proof that the distribution orthogonal to the constant-task fibers is globally integrable, governed by an exact global logarithmic potential field. This potential function enables a complete topological classification of the kinetic space into  $2^n - 2$  transitional and 2 extremal orthants based on the signature w.r.t. the null-space generator of the linear part of the signed-quadratic actuation map. The transitional orthants are then further grouped in  $n - 1$  layers,  $\mathcal{L}_l$  with  $l = 1, \dots, n - 1$ , containing each  $\binom{n}{l}$  orthants. The orthogonal foliation acts like a ‘wavefront’ of section orthogonal to all the fibers, which starts from an extremal orthant, goes through the transitional layers and ends in the other extreme orthant. Through this geometric framework,



(a) Pseudo-inverse vs orthogonal allocation in extremal sections ( $\mathcal{L}_0, \mathcal{L}_3$ )



(b) Pseudo-inverse vs orthogonal allocation in transitional sections ( $\mathcal{L}_1, \mathcal{L}_2$ )

Fig. 6: Geometric and topological comparison of the classical pseudo-linear allocator versus the orthogonal foliation ( $n = 3, m = 2$ ).

(a) The pseudo-linear allocation manifold (red surface) exhibits non-linear deformation in the kinetic space  $\mathcal{V}$ . It is intrinsically fractured by  $2^n - 2 = 6$  orthant boundaries (dashed red lines) radiating from the origin. In contrast, the extremal orthogonal sections ( $\mathcal{L}_0$  and  $\mathcal{L}_3$ , blue surfaces) smoothly embed the preimage of a circular task-space region (closed curves) without a single boundary intersection, visually confirming their property as global diffeomorphisms.

(b) The pseudo-linear manifold (red) overlaid with a transitional orthogonal section. At points of intersection, the stark misalignment of their tangent spaces visually demonstrates the failure of the pseudo-linear mapping to maintain orthogonality with the fibers. Furthermore, the orthogonal section is partitioned by only  $\binom{n}{1} = n = 3$  precise coordinate plane intersections (solid black lines, the hinges), halving the singular fragmentation of the baseline.

some structural limitations of classical pseudo-inverse allocation are systematically highlighted. Pseudo-linear methods distribute their mappings across an exponential ( $2^n - 2$ ) number of transitional orthants, forcing trajectories to cross  $(n - 1)$ -dimensional boundary hyperplanes and triggering infinite-derivative kinetic singularities. In contrast, transitional orthogonal sections partition the space based on combinatorial

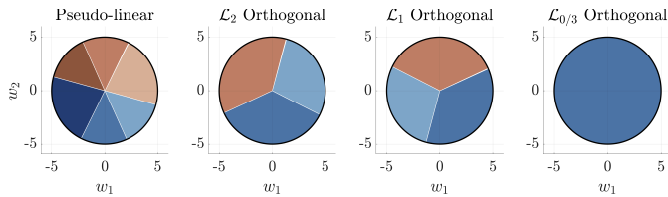


Fig. 7: Task space  $\mathcal{W}$  sector divisions in orthant switching

Fig. 8: Combinatorial reduction of task space partitions. Four identical circular regions in the task space  $\mathcal{W}$  show how the different allocation maps partition the task space. Left: The pseudo-linear allocator fractures the task space into  $2^n - 2 = 6$  narrow sectors. Middle: The  $\mathcal{L}_1$  and  $\mathcal{L}_2$  transitional orthogonal allocators structurally expand the feasible volumes, reducing the partition to exactly  $n = 3$  larger sectors each. Right: The extremal orthogonal allocator ( $\mathcal{L}_0$  or  $\mathcal{L}_3$ ) completely unifies the mapping, yielding a single, unpartitioned operational domain spanning the entire circle.

scaling  $\binom{n}{l}$ . For adjacent layers ( $l = 1$  or  $l = n - 1$ ), this partitions the space linearly ( $n$ ), significantly improving the coverage of the task space and reducing the frequency of boundary crossings. However, the mathematical analysis also reveals a trade-off: the kinetic singularities encountered at these orthogonal boundaries exhibit a more severe divergence compared to the pseudo-inverse mapping. On the contrary, orthogonal sections in extremal orthants have distinct topological advantages shown by the analysis. Because the orthogonal manifolds within these extremal regions form a global diffeomorphism to the entire task space without singular boundary intersections, they yield a static control allocator that intrinsically guarantees the avoidance of both geometric rank-loss and temporal kinetic singularities.

Ultimately, this work frames redundancy resolution for signed-quadratic systems as a fundamental problem of manifold selection rather than purely constrained numerical optimization. The established geometric framework provides a rigorous theoretical basis for static allocation.

This theoretical work can pave the way for a new generation of control methods for any real system subject to a signed-quadratic type of actuation, such as, e.g., multi-rotor aerial systems, propeller-based underwater and marine vehicles.

Future work will leverage these exact topological characterizations to design global null-space projection strategies, integrating strict physical torque saturation limits and energy-minimization objectives directly into the native geometry of the orthogonal foliation.

## IX. ACKNOWLEDGEMENTS

The authors thank their colleagues, mentors, and mentees for inspiring discussions. The authors also acknowledge the LLM Gemini 3 (early 2026) for assistance in proofreading and optimizing the data processing and plotting scripts. The functionality of all code and the accuracy of the resulting outputs were manually verified by the authors.

## REFERENCES

[1] T. A. Johansen and T. I. Fossen. “Control allocation—A survey”. In: *Automatica* 49.5 (2013), pp. 1087–1103.

[2] W. C. Durham. “Constrained control allocation”. In: *Journal of Guidance, Control, and Dynamics* 16.4 (1993), pp. 717–725.

[3] D. Enns. “Control allocation approaches”. In: *AIAA Guidance, Navigation, and Control Conference*. AIAA Paper 1998-4109. Boston, MA, 1998.

[4] M. Bodson. “Evaluation of Optimization Methods for Control Allocation”. In: *Journal of Guidance, Control, and Dynamics* 25.4 (2002), pp. 703–711.

[5] O. Härkegård. “Backstepping and Control Allocation with Applications to Flight Control”. PhD thesis. Linköping, Sweden: Linköping University, 2003.

[6] O. Härkegård and S. T. Glad. “Resolving actuator redundancy—optimal control vs. control allocation”. In: *Automatica* 41.1 (2005), pp. 137–144.

[7] D. A. Santos and J. A. Bezerra. “On the control allocation of fully actuated multirotor aerial vehicles”. In: *Aerospace Science and Technology* 122 (2022), p. 107424.

[8] L. Zaccarian. “Dynamic allocation for input redundant control systems”. In: *Automatica* 45.6 (2009), pp. 1431–1438.

[9] D. O. Sighthorsson, A. Serrani, S. Yurkovich, M. A. Bolender, and D. B. Doman. “Tracking control for an overactuated hypersonic air-breathing vehicle with steady state constraints”. In: *Proceedings of the AIAA Guidance, Navigation, and Control Conference and Exhibit*. 2006, pp. 1–17.

[10] A. Serrani. “Output regulation for over-actuated linear systems via inverse model allocation”. In: *Proceedings of the 51st IEEE Conference on Decision and Control (CDC)*. 2012, pp. 4871–4876.

[11] A. Cristofaro, S. Galeani, and A. Serrani. “Output invisible control allocation with asymptotic optimization for nonlinear systems in normal form”. In: *Proceedings of the 56th IEEE Conference on Decision and Control (CDC)*. 2017, pp. 2563–2568.

[12] R. Masocco, L. Tarantino, S. Galeani, and M. Sassano. “A dynamic optimization approach to steady-state input allocation for nonlinear redundant systems”. In: *2024 10th Int. Conf. on Control, Decision and Information Technologies*. 2024, pp. 2833–2838.

[13] S. Akbari, S. Galeani, G. Manca, and M. Sassano. “Dynamic Control Allocation for Nonlinear Systems via a Sensitivity Approach”. In: *IEEE Control Systems Letters* 9 (2025), pp. 2549–2554.

[14] A. Cristofaro and T. A. Johansen. “Fault tolerant control allocation using unknown input observers”. In: *Automatica* 50.7 (2014), pp. 1891–1897.

[15] J. Cai and M. Lovera. “An Active Fault-Tolerant Online Control Allocation Scheme for a Dual-System UAV in Transition Flight”. In: *arXiv preprint arXiv:2510.04853* (2025).

[16] L. Govoni and A. Cristofaro. “Control allocation for windup mitigation in weakly redundant systems with input saturation”. In: *IEEE Control Systems Letters* 7 (2023), pp. 3295–3300.

[17] D. Brescianini and R. D’Andrea. “An omni-directional multirotor vehicle”. In: *Mechatronics* 55 (Nov. 2018), pp. 76–93.

[18] S. Park, J. Lee, J. Ahn, M. Kim, J. Her, G.-H. Yang, and D. Lee. “ODAR: Aerial Manipulation Platform Enabling Omnidirectional Wrench Generation”. In: *IEEE/ASME Transactions on Mechatronics* 23.4 (2018), pp. 1907–1918.

[19] M. Hamandi, K. Sawant, M. Tognon, and A. Franchi. “Omni-Plus-Seven (O7+): An Omnidirectional Aerial Prototype with a Minimal Number of Uni-directional Thrusters”. In: *2020 International Conference on Unmanned Aircraft Systems (ICUAS)*. Athens, Greece, 2020, pp. 754–761.

[20] H. Lee, S. Cheng, Z. Wu, J. Lim, R. Siegart, and N. Hovakimyan. “Geometric Tracking Control of Omnidirectional Multirotors for Aggressive Maneuvers”. In: *IEEE Robotics and Automation Letters* 10.2 (2025), pp. 1130–1137.

[21] P. Shu, F. Li, J. Zhao, and M. Oya. “Robust Adaptive Control for A Novel Fully-Actuated Octocopter UAV with Wind Disturbance”. In: *Journal of Intelligent & Robotic Systems* 103.1 (2021), p. 6.

[22] M. Á. Trujillo, J. R. Martínez-de Dios, C. Martín, A. Viguria, and A. Ollero. “Novel Aerial Manipulator for Accurate and Robust Industrial NDT Contact Inspection: A New Tool for the Oil and Gas Inspection Industry”. In: *Sensors* 19.6 (2019), p. 1305.

[23] A. Yiğit, M. A. Perozo, L. Cuvillon, S. Durand, and J. Gangloff. “Novel omnidirectional aerial manipulator with elastic suspension: Dynamic control and experimental performance assessment”. In: *IEEE Robotics and Automation Letters* 6.2 (2021), pp. 612–619.

- [24] R. Rashad, J. Goerres, R. Aarts, J. B. C. Engelen, and S. Stramigioli. “Fully Actuated Multirotor UAVs: A Literature Review”. In: *IEEE Robotics & Automation Magazine* 27.3 (2020), pp. 97–107.
- [25] M. Hamandi, Q. Sablé, M. Tognon, and A. Franchi. “Understanding the omnidirectional capability of a generic multi-rotor aerial vehicle”. In: *IEEE Workshop on Aerial Robotic Systems Physically Interacting with the Environment (AIRPHARO)*. 2021.
- [26] M. Hamandi, F. Usai, Q. Sablé, N. Staub, M. Tognon, and A. Franchi. “Design of multirotor aerial vehicles: A taxonomy based on input allocation”. In: *The International Journal of Robotics Research* 40.8-9 (2021), pp. 1015–1044.
- [27] Y. Aboudorra, C. Gabellieri, R. Brantjes, Q. Sablé, and A. Franchi. “Modelling, Analysis, and Control of OmniMorph: an Omnidirectional Morphing Multi-rotor UAV”. In: *Journal of Intelligent and Robotic Systems* 110.21 (2024), pp. 1–21.
- [28] M. Zhao, K. Kawasaki, T. Anzai, X. Chen, K. Okada, and M. Inaba. “Transformable multirotor with two-dimensional multilinks: Modeling, control, and whole-body aerial manipulation”. In: *The International Journal of Robotics Research* 37.9 (2018), pp. 1085–1112.
- [29] R. Oung and R. D’Andrea. “The Distributed Flight Array: Design, implementation, and analysis of a modular VTOL vehicle”. In: *The International Journal of Robotics Research* 33.3 (2013), pp. 375–400.
- [30] K. Garanger, T. Khamvilai, J. Epps, and E. Feron. *The Dodecopter: a Versatile Multirotor System of Dodecahedron-Shaped Modules*. <https://arxiv.org/abs/2504.16475>. arXiv preprint. 2025.
- [31] M. Kamel, K. Alexis, M. Achtelik, and R. Siegwart. “Fast nonlinear model predictive control for multicopter attitude tracking on  $SO(3)$ ”. In: *2015 IEEE Conference on Control Applications (CCA)*. IEEE, 2015, pp. 1160–1166.
- [32] A. Baldini, R. Felicetti, A. Freddi, S. Longhi, and A. Monteriù. “Fault Tolerant Control for Tilted Hexarotors Under a Rotor Failure”. In: *22nd IFAC World Congress*. Vol. 56. 2. Yokohama, Japan, July 2023, pp. 2486–2493.
- [33] F. Liao, K. Peng, E. Wei, W. Leong, and D. Neo. “Active fault tolerant control for multirotor UAVs: Controllability, design and experiment”. In: *Control Engineering Practice* 164 (2025), p. 106497.
- [34] T. I. Fossen. *Handbook of Marine Craft Hydrodynamics and Motion Control*. John Wiley & Sons, 2011.
- [35] G. Antonelli. *Underwater Robots*. 4th. Springer, 2018.



**Antonio Franchi** (F’23–SM’16–M’07) received the Ph.D. degree in system engineering from the Sapienza University of Rome, Rome, Italy in 2010, and the HDR degree in Science, from the National Polytechnic Institute of Toulouse in 2016. From 2014 to 2019 he was a tenured CNRS researcher at LAAS-CNRS, Toulouse, France. Since 2019 is with the University of Twente, Enschede, The Netherlands where is currently Full Professor in aerial robotics control. Since 2023 he is also Full Professor in the Department of Computer, Control and

Management Engineering at Sapienza University of Rome. He co-authored more than 190 publications in peer-reviewed international journals, books, and conferences on design, control, and estimation for robotic systems applied to multi-robot systems and aerial robots.